JGR Planets

RESEARCH ARTICLE
10.1029/2025JE009107

Special Collection:
The Mars 2020 Perseverance Rover's Exploration of the Jezero Crater Margin and Neretva Vallis

In Situ Carbonation of Sedimentary and Igneous Rocks of Ultramafic Composition in Jezero Crater, Mars

E. Clavé[1,2], O. Beyssac[3], P. Beck[4], C. Royer[5], L. Mandon[4], N. Mangold[6], O. Forni[7], E. Dehouck[2], C. Bedford[8], A. Udry[9], S. Schröder[1], S. Bernard[3], C. Quantin-Nataf[2], M. Loche[7], J. Aramendia[10], A. Brown[11], G. Caravaca[12], E. Cardarelli[13], L. Coloma[10], S. A. Connell[8], T. Fouchet[14], J. R. Johnson[15], G. Lopez-Reyes[16], J. M. Madariaga[10], J. A. Manrique[17], S. Maurice[7], P.-Y. Meslin[7], S. Le Mouélic[6], A. M. Ollila[17], P. Pilleri[7], C. Pilorget[18,19], K. Rammelkamp[1], F. Seel[1], J. I. Simon[20], U. Wolf[17], A. Zastrow[17], S. Clegg[17], O. Gasnault[7], R. C. Wiens[8], and A. Cousin[7]

[1]Deutsches Zentrum für Luft- und Raumfahrt e.V. (DLR), Institute of Space Research, Berlin, Germany, [2]Université Claude Bernard Lyon 1, ENS de Lyon, CNRS, UJM, LGL-TPE, UMR 5276, Villeurbanne cedex, France, [3]Institut de Minéralogie, de Physique des Matériaux et de Cosmochimie, CNRS UMR 7590, Sorbonne Université, Muséum National d'Histoire Naturelle, Paris, France, [4]Université Grenoble-Alpes, CNRS, IPAG, UMR 5274, Grenoble, France, [5]LATMOS/IPSL, UVSQ Université Paris-Saclay, Sorbonne Université, CNRS, Guyancourt, France, [6]Nantes Université, University Angers, CNRS, UMR 6112, Laboratoire de Planétologie et Géosciences, Nantes, France, [7]Institut de Recherche en Astrophysique et Planétologie, CNRS, Université de Toulouse, UPS-OMP, Toulouse, France, [8]Earth, Atmospheric, and Planetary Sciences, Purdue University, West Lafayette, IN, USA, [9]Department of Geoscience, University of Las Vegas, Las Vegas, NV, USA, [10]Department of Analytical Chemistry, University of the Basque Country UPV/EHU, Leioa, Spain, [11]Plancius Research, Manlius, NY, USA, [12]Laboratoire Géosciences Environnement Toulouse, UMR 5563 CNRS, IRD, CNES, Université de Toulouse, Toulouse, France, [13]Department of Earth, Planetary, and Space Sciences, University of California Los Angeles, Los Angeles, CA, USA, [14]LIRA, Observatoire de Paris, Université PSL, CNRS, Sorbonne Université, Université Paris Cité, Meudon, France, [15]Johns Hopkins University Applied Physics Laboratory, Laurel, MD, USA, [16]Research Group ERICA, Department of Applied Physics, Universidad de Valladolid, Valladolid, Spain, [17]Los Alamos National Laboratory, Los Alamos, NM, USA, [18]Institut d'Astrophysique Spatiale/Université Paris-Saclay/CNRS, Orsay cedex, France, [19]Institut Universitaire de France, Paris, France, [20]NASA Johnson Space Center, Houston, TX, USA

Abstract Over 3.5 years of exploration in Jezero Crater, the Perseverance rover has explored several geological units of diverse origins and natures, performing multi-technique remote analyses of the chemistry and mineralogy of rocks with the SuperCam instrument suite. Three of these units are dominated by mafic to ultramafic rocks: the igneous rocks of Séítah (olivine cumulate on the crater floor), the sedimentary rocks of the Upper Fan (Western delta) and the Margin Unit, of likely igneous origin. Despite their diverse natures, these three different units present similar mineralogical assemblages with: (a) primary igneous minerals (olivine, pyroxene, Cr-rich Ti-Fe oxides), (b) Fe-Mg carbonate, (c) hydrated/hydroxylated silica, and (d) phyllosilicates. The abundance of carbonate is variable, and we estimate it around 3–9 wt.% and up to 6–16 wt.% carbonate mineral in the Upper Fan and Margin Unit, respectively. We propose that most of these carbonates formed through in situ carbonation of mafic/ultramafic material, whether these rocks were emplaced through igneous or sedimentary processes. The distribution of carbonate with elevation in the Upper Fan and Margin Unit suggests a contribution of the lacustrine activity to the carbonate process, possibly enhanced by hydrothermal activity. These in situ observations may be extrapolated to other carbonates-bearing rocks on Mars and would make the amount of carbon potentially stored in Martian ultramafic rocks overall significant. This would suggest that carbonation of ultramafic rocks might have played a key role in pumping CO_2 from and therefore in cooling the Martian atmosphere.

Plain Language Summary Over 3.5 years of exploration in Jezero Crater, the Perseverance rover has explored several geological units of diverse origins. Despite different natures (sedimentary or magmatic), three of these units share a lot of common characteristics (composition, mineralogy, texture, …). These three units show evidence of alteration of the rocks through interaction with liquid water. The nature and extent of this alteration shows a relation with the water level of an ancient lake in the crater.

Key Points:

- A similar mineralogical assemblage is found in igneous rocks in the crater floor, sedimentary rocks in the Upper Fan and in the Margin Unit
- There is evidence of olivine alteration to Fe-Mg carbonates and hydrated silica in these three units
- Differences in alteration states along the traverse could be related to elevation with respect to lake level

Supporting Information:

Supporting Information may be found in the online version of this article.

Correspondence to:
E. Clavé,
elise.clave@univ-lyon1.fr

Citation:
Clavé, E., Beyssac, O., Beck, P., Royer, C., Mandon, L., Mangold, N., et al. (2026). In situ carbonation of sedimentary and igneous rocks of ultramafic composition in Jezero Crater, Mars. *Journal of Geophysical Research: Planets*, *131*, e2025JE009107. https://doi.org/10.1029/2025JE009107

Received 1 APR 2025
Accepted 30 MAR 2026

1. Introduction

Carbonate-rich rocks constitute a valuable marker of fluid-rock interactions, such as chemical alteration of rocks and/or precipitation from fluids. Carbonate phases record information about the chemical composition, pH, and temperature of the past fluids in which they formed, which can be decrypted through textural and geochemical analyses (e.g., Kelemen et al., 2011). On Mars, depending on their formation process, carbonates can inform us of past climatic conditions, or about past hydrothermal systems, which are key environments for astrobiology (e.g., Bridges et al., 2019; Niles et al., 2013; Scheller et al., 2021). Moreover, carbonates on Earth are intimately associated with life: a large portion of terrestrial carbonates have a direct biotic origin (Shields, 2007). Martian carbonates are thus targets of interest in the search for past life on Mars (e.g., Benzerara et al., 2018; Bosak et al., 2021; Farmer & Des Marais, 1999). Finally, despite the fact that carbonates may have trapped (or released) carbon from (or into) the atmosphere over geological time and therefore impacted Martian climate (Edwards & Ehlmann, 2015; Lammer et al., 2013; Manning et al., 2006), there is an apparent scarcity of carbonates at the surface of Mars based on orbital observation, resulting in a "missing carbon" paradox (Bibring et al., 2005; Morris et al., 2010). This paradox may be explained by a detectability issue, but may also result from a massive dissolution of carbonates that has yet to be understood (Gaillard et al., 2013). The loss of some carbon to space may explain the low modern carbon inventory (Jakosky et al., 2018; Lammer et al., 2013). However, the numerous traces of past liquid water activity at the surface of Mars in the first billion year require either a continuous greenhouse effect, enabled by a denser, possibly CO_2-dominated atmosphere (Kite et al., 2021), or that impact or volcanic events enabled episodic liquid flows in otherwise icy conditions (Kite et al., 2017; Ramirez & Craddock, 2018; Wordsworth et al., 2018). Assuming the presence of such a thicker, CO_2-rich atmosphere, it should have led to the formation of carbonates following for instance fluid-rock interactions.

Carbonates have been detected on the surface of Mars from orbit with instruments like MGS/TES, Mars Express/OMEGA, MRO/CRISM in bedrock in various regions, including exceptionally frequent exposures of carbonate-rich rocks in the Nili Fossae region (Carter et al., 2023; Ehlmann et al., 2008; Mandon et al., 2020). Beside the Nili Fossae region, carbonates were in particular observed in the context of deep Martian crust exposures, for example, in association with craters exposing Noachian rocks (Michalski & Niles, 2010; Viviano-Beck et al., 2014; Wray et al., 2016), and as part of weathering profiles in late Noachian terrains (Bultel et al., 2019), but overall in spatially limited outcrop exposures. Carbonates were also detected in the landing sites of several in situ missions. First, at the Phoenix landing site (Ca-carbonate in soils, 3–5 wt.%; Boynton et al., 2009), and the Columbia Hills of Gusev Crater explored by the MER Spirit rover (an outcrop rich in Fe-Mg carbonate, 16–34 wt.%; Morris et al., 2010). In Gale crater, explored by the Curiosity rover, Fe-Mg carbonates were detected by the SAM mass spectrograph in the regolith (Leshin et al., 2013); Fe-rich carbonate was detected in minor amount within the Glen Torridon clay-rich unit, and siderite was firmly identified by the CheMin X-ray diffractometer within the so-called "marker-band" of the sulfate-bearing unit (Burtt et al., 2024; Thorpe et al., 2022; Tutolo et al., 2025). Finally, Fe-Mg carbonates were characterized on the floor of Jezero Crater by the Perseverance rover (Clavé et al., 2023; Corpolongo et al., 2023; Mandon et al., 2023; Tice et al., 2022), as well as in the sedimentary rocks of the Western Fan (e.g., Dehouck et al., 2024; Royer et al., 2025; Tice et al., 2024). Carbonates have also been identified and characterized in several Martian meteorites, especially ALH84001 and NWA7533, but a Martian—as opposed to terrestrial—origin of the carbonates has been questioned (Bridges et al., 2019; Halevy et al., 2011; Niles et al., 2013).

The detection of carbonate mineral phases from orbit was critical in supporting the choice of Jezero Crater as a landing site for the Mars 2020 mission. Indeed, this Noachian-aged crater lies within the largest carbonate-rich unit detected on Mars from orbit (Brown et al., 2020; Ehlmann et al., 2008; Goudge et al., 2015; Horgan et al., 2020; Mandon et al., 2020; Tarnas et al., 2021). Carbonates observed from orbit in Jezero Crater are found in diverse lithologies, and may have formed through different geological and aqueous processes, which are challenging to characterize based on orbital data alone. Since landing on the crater floor of Jezero Crater in February 2021, Perseverance has explored the main carbonate-bearing units within the crater and characterized them with its scientific payload. Surface analyses rely on two complementary approaches. Remote sensing is performed with Mastcam-Z multi-spectral stereo imaging system (Bell et al., 2021) and SuperCam (Maurice et al., 2021; Wiens et al., 2021). Proximity science relies on PIXL X-ray fluorescence micro-mapper (Allwood et al., 2020) and SHERLOC deep UV micro Raman (Bhartia et al., 2021). One of the main goals of the Mars 2020 mission is the identification, characterization and collection of rock cores to be returned to Earth as part of the Mars Sample Return (MSR) program, to enable more detailed analyses in the laboratory. Here we use multi-

technique data acquired in situ with SuperCam to characterize the diversity of carbonates in Jezero Crater, observed in both sedimentary and igneous rocks, and constrain their formation processes.

2. Materials and Methods

2.1. The SuperCam Instrument

This study focuses on data acquired with SuperCam with three spectroscopy techniques on rocks located several meters from the instrument: laser-induced breakdown spectroscopy (LIBS), Raman spectroscopy, and visible and infrared reflectance (VISIR) spectroscopy. SuperCam is also equipped with a remote micro-imager (RMI) providing color context images. Details about the instrument and the associated techniques are provided elsewhere (Maurice et al., 2021; Wiens et al., 2021).

The Nd:YAG laser uses 1,064 nm pulses to excite LIBS plasmas. The same laser can also be operated at 532 nm through the use of a second-harmonic generator for Raman spectroscopy. The laser pulse duration is 3–4 ns and the repetition rate is 3 Hz for LIBS and 10 Hz for Raman. For both techniques, the emitted/scattered light is collected by a 110 mm diameter telescope and transferred to the SuperCam spectrometers through a bundle of optical fibers. SuperCam is equipped with four spectrometers covering different spectral ranges. Three of these spectrometers are used for LIBS and visible reflectance spectroscopy (VIS): 243.7–345.0 nm, 379.0–465.0 nm, and 532.0–858.8 nm (Wiens et al., 2021), only the latter is used for Raman analyses. The fourth spectrometer, dedicated to near-infrared reflectance spectroscopy (IRS) covers the range 1.3–2.6 μm (Fouchet et al., 2022).

The spectroscopy techniques and RMI images are co-aligned, enabling a single selected point on a Martian target to be characterized by LIBS for elemental analysis, as well as Raman and VISIR for mineralogy, although the analytical footprints are of different sizes (values for targets between 1.5 and 6 m): ∼0.20–0.45 mm in diameter for LIBS; 1.0–4.2 mm for Raman and VIS (0.7 mrad); 1.8–6.9 mm for IRS (∼1.15 mrad). The field of view of the RMI is 18.8 mrad with an effective image resolution better than 0.050 mrad corresponding to <0.24 mm at 3 m (Maurice et al., 2021).

To get representative information from generally heterogeneous rocks, spectra are typically acquired in series of 5–10 points, forming a linear raster or a grid. Two or three RMI images are usually acquired to provide context and textural information on the target, as well as to document changes due the laser shots. The RMI images are then assembled into mosaics. On each point, one or several of SuperCam's spectroscopy techniques can be used. LIBS generally comes first, because the shock-wave induced by the plasma expansion cleans the dust from the target's surface, reducing the contribution of dust to the VISIR and/or Raman spectra acquired afterward (Maurice et al., 2021; Sharma et al., 2007). On each raster point, 30 laser shots are generally fired for LIBS. All single-shot spectra are returned, but the spectra corresponding to the first five shots, which often sample the dust (Lasue et al., 2018; Maurice et al., 2016; Meslin et al., 2013), are not considered for the average spectrum of each point. Raman spectra are typically acquired accumulating the data over 100 to 400 laser shots and with a gate opening of the detector of 100 ns. Depending on the time of day and temperature of the instrument, IRS preset integration times are 30–205 ms per spectral channel, and 256 spectral channels are acquired over the 1.3–2.6 μm range.

2.2. Remote Micro Imager (RMI)

The SuperCam remote micro-imager (RMI) was presented in Gasnault et al. (2021). In this study, RMIs and other context images acquired by cameras onboard the rover are used to filter out targets corresponding to loose material (soil, drill tailings) and rocks that are not in place. The analysis can thus focus on bedrock only along the rover traverse. Loose material is easily identified within RMI images taken before and after LIBS measurements, and other cameras with wider fields of view provide the context to support the selection of bedrock. SuperCam observation points are located precisely in the RMI images for each technique. It is therefore even possible to select the points of interest on a given rock, and identify those on the bulk rock versus secondary and/or diagenetic phases.

2.3. LIBS Data Processing

All LIBS spectra are subjected to a series of pre-processing steps, as part of a standardized pipeline. These different pre-processing steps are presented elsewhere (R. Anderson et al., 2022).

2.3.1. Major Oxide Composition (MOC)

Empirical quantification models were developed to derive the concentration of major elements most relevant in geochemistry from LIBS data: SiO_2, TiO_2, Al_2O_3, FeO(T), MgO, CaO, Na_2O, K_2O. These were trained on an extensive laboratory database acquired on samples of variable chemical compositions and with the flight instrument at the Los Alamos National Laboratory (LANL) in experimentally simulated Martian atmospheric conditions. General averaged one-sigma accuracies for SiO_2, TiO_2, Al_2O_3, FeO(T), MgO, CaO, Na_2O, K_2O are ±6.1, 0.3, 1.8, 3.1, 1.1, 1.3, 0.5 and 0.6 wt.% respectively (Anderson et al., 2022). Mg# are computed from molar elemental compositions, as $Mg/(Fe + Mg) * 100$.

The first step looking for carbonate-compatible compositions is based on the MOC. The eight major elements quantified with the SuperCam MOC presented above do not enable direct identification of carbonates. However, they give indications, and many points can already be ruled out as being significantly carbonate-bearing based on the MOC only. In particular, carbonate-bearing points must have a lower SiO_2 content than any silicate; we therefore use a threshold of 30 wt.% SiO_2 (justified further in Text S1 and Figure S1 of Supporting Information S1) and only look for carbonates in points with a silica content lower than this threshold.

2.3.2. Identifying Carbon Enhancement Related to Carbonates in LIBS Spectra

The characterization of the carbon signal from LIBS data in this study is inspired by the approaches presented in (Beck, Meslin, et al., 2024; Clavé et al., 2023). Similarly to these studies, the challenge is to account for the contribution of the atmospheric CO_2, and identify an excess carbon signal corresponding to carbonate in the target. The strategy to that end relies on normalization of the carbon signal to the oxygen signal (Beck et al., 2016; Gasnault et al., 2012; details in Supporting Information S1 file: Text S1 and associated Figures and Tables).

Based on a literature search and the specific constraints of SuperCam (spectral range, calibration; detailed in Table S1 of Supporting Information S1), we decided to use three carbon lines in this study: C II 658 nm, C II 678 nm and C II 723 nm (a doublet), and one oxygen line: the O I 777 nm triplet (unresolved). Each of these lines is fitted with a pseudo-Voigt model together with a linear function as the local baseline using the lmfit package in Python (Newville et al., 2025). For each line, we identified a set of interfering lines to fit with additional pseudo-Voigt profiles, to reduce interference from other elements in the characterization of the carbon and oxygen signals (detailed in Table S2 and Figure S2 of Supporting Information S1).

Because the ionization degree of the carbon and oxygen lines used here are different (C II and O I), variations of irradiance with varying distance to targets will impact the C-to-O ratio (Schröder et al., 2019). To account for this distance effect, targets are binned per distance and normalized to standard deviation within each bin (details in Text S1 and Figure S3 of Supporting Information S1).

Based on observations of the SuperCam Calibration Targets (SCCTs) (detailed in Text S1 and Figures S4–S6 of Supporting Information S1), we chose to use criteria on the normalized C/O values to identify an excess of carbon compared to the atmospheric contribution. Consequently, we identify a point as carbonate-bearing when: (a) the SiO_2 content in this point is below 30 wt.%; (b) two out of the three considered carbon lines have normalized C/O values higher than 1.27 (threshold fixed based on distribution following the Student test, for a 10% risk of false positives, as in Clavé et al., 2023). These are very conservative criteria, which should yield some false negatives but minimal false positives (Figure S6 in Supporting Information S1 for performances on SCCTs).

2.3.3. Stoichiometric Analyses for Identification of Primary Silicates Based on the MOC

To identify olivine in the LIBS data set, with stoichiometric analyses, we use similar strategies as in previous studies based on SuperCam LIBS data (Beyssac et al., 2023, 2026; Udry et al., 2023, 2024). Olivine is identified with: 3 (±0.2) total cations with 4 O; $1.5 < (Fe + Mg)/Si < 2.0$; $Al/Si < 0.12$; $Na/Si < 0.05$; Totals ≥ 85 wt.%; $2.8 <$ Total cations < 3.2. To confirm the detection of a stoichiometric olivine, the stoichiometric criteria listed above must be met by: (a) the mean composition of the point computed in the standard way from the MOC (average of 25 laser shots); (b) the composition individually derived from at least 12 of the shots acquired on that point. We can only identify single minerals that have a larger grain size than that of the LIBS spot size, resulting in likely under predictions.

Pyroxenes were also detected based on the LIBS data using a similar strategy (Beyssac et al., 2026), namely Mg-rich orthopyroxene to low-Ca pigeonite. We focus here on olivine as it is by far the dominant igneous mineral in these rocks, and because it alters much faster compared to low Ca pyroxene (Kelemen, 2020).

2.3.4. Spectral Unmixing for Semi-Quantitative Characterization of Major and Minor Elements

Spectral Unmixing (SU) belongs to the family of calibration-free LIBS (Hermann et al., 2023; Poggialini et al., 2023) and derives semi-quantitative elemental abundances directly from LIBS spectral data, without the need for reference measurements of laboratory standards and calibration models (Hansen, 2022; Schröder et al., 2024). In this approach, an experimental LIBS spectrum is matched with a linear combination of element-wise simulated LIBS spectra. The obtained coefficients for each element are called SU scores and provide semi-quantitative information about elemental abundances. More details about the SU method can be found in the Supporting Information (Text S2 in Supporting Information S1).

We use the SU scores to look for local enhancement in various minor elements. All LIBS spectra acquired with SuperCam on targets within 6 m were fitted and SU scores derived for all elements. The SU scores were normalized to the maximum value per element, to study relative variations along the traverse. Because of the specific challenges of hydrogen characterization and to reduce the influence of distance on the hydrogen signal (Rapin et al., 2017; Schröder et al., 2015), the H score was normalized to the O score. We looked for local enhancements in H, Mn, Cr, S but also Ni, Sr, …. We also looked into the Ti score, as the MOC tends to underestimate high Ti contents (R. Anderson et al., 2022).

2.3.5. Using the MOC to Identify and Filter Out Coating Observations

Many rock surfaces in Jezero Crater are partially or fully covered with a relatively thick (hundreds of microns to millimeters) indurated coating that prevents SuperCam observation of the underlying rock in those locations. The coating's composition appears similar across the various rocks observed along the traverse, being somewhat close to that of aeolian dust (Garczynski, Ollila, et al., 2025). Based on the various observations of the MOC data from the Margin Unit, we identified a typical coating composition (Figure S8 in Supporting Information S1). This coating is interpreted as a late alteration feature, and its composition is not correlated to the substrate composition. Moreover, this coating does not contain carbonate to an amount sufficient that it can be detected with SuperCam or relevant for this study. We therefore consider that it does not hold information relevant to the formation of the carbonate-bearing rocks or the carbonates themselves. Instead these coatings make it more challenging to interpret variations in composition or carbonate distribution along the traverse. Thus we identify the coating observations and remove them from the data set we use in this study. To do so, we use thresholds on the MOC data, determined on coating observations confirmed based on visual check in the RMIs: SiO_2 between 40 and 50 wt.%; Al_2O_3 between 7.0 and 12.5 wt.%; TiO_2 between 0.6 and 1.1 wt.%; FeOT between 10.0 and 15.0 wt.% (Figure S8 in Supporting Information S1). The distribution of coating identifications based on these criteria along the traverse is shown in Figure S9 of Supporting Information S1. Note that this approach only works for pure coating analyses; for observations that sample part coating and part rock, the composition of the coating will affect the resulting composition, but these can not be filtered using the above approach, so some coating contribution likely remain in the data set.

2.4. VISIR Data Processing

Acquired VIS and IR spectra were calibrated into reflectance using standardized pipelines, presented in Mandon et al. (2023) and Royer et al. (2023), respectively. Raw VIS spectra (50 for each points) were averaged and converted to relative reflectance using (a) an instrument transfer function derived from lab measurements, (b) division by a radiance spectrum of the white SCCT (Cousin et al., 2022), and (c) multiplication by Mars-to-Sun distance and solar incidence cosine ratios. Calibration of the IRS data uses a separate pipeline, which includes dark smoothing and subtraction, conversion to reflectance using pre-flight and white SCCT measurements, removal of artifacts, and empirical correction of the atmospheric CO_2 lines. As the VIS and IR ranges are covered by two spectrometers with different calibration procedures, and these observations have slightly different field-of-view, comparing associated data should be made with caution. The VIS part of the spectra is smoothed with a Savitsky-Golay filter (windows of 101 and 51), whereas the IR part is used with no smoothing, similar to previous studies (e.g., Mandon et al., 2024).

2.4.1. Spectral Parameters for Global Observations of IRS Data

In order to investigate spectral variations across the rover transect, several spectral parameters were used. They are derived from those defined by Viviano-Beck et al. for CRISM data (Viviano-Beck et al., 2014), and adapted to SuperCam IRS specific spectral sampling. We use four such spectral parameters in this study:

1. A slope parameter in the 1.35–1.80 μm range to trace the high wavelength side of Fe^{2+} absorption in olivine or Fe-bearing carbonates.
2. The 2.2 μm band depth to trace Si-OH or Al-OH (band center at 2.210 μm, shoulders at 2.165 and 2.250 μm);
3. The 2.3 μm band depth to trace Mg-OH or carbonates (band center at 2.320 μm, shoulders at 2.230 and 2.390 μm)
4. The 2.5 μm band depth to trace carbonate (band center 2.530 μm, shoulders at 2.390 and 2.570 μm);

To look for carbonate-consistent spectra in the data set, we also use the minimum of the 2.3 and 2.5 band depth values.

2.4.2. Band Fitting With Multi Gaussian Modeling to Characterize Carbonates

In this study, the absorption bands we focus on are those that can be attributed to carbonates (CO_3 group). These bands are automatically extracted from each spectrum using a method based on spectral continuum removal and fitting through the linear combination of multiple Gaussians (Multi Gaussian Modeling—MultiGM, described in detail by Royer et al., 2025). This method allows for determining the band minimum position, band depth, and the band depth to noise ratio (BDNR), a metric used to filter detections, keeping only the most certain ones. Carbonates are typically identified by a pair of absorption bands around 2.3 and 2.5 μm, attributed to CO_3 in carbonates. Due to the ubiquitous presence of phyllosilicates in Jezero Crater, most VISIR spectra acquired with SuperCam show a 2.35 μm absorption (e.g., Mandon et al., 2023; Royer et al., 2025), which is thus not discriminating for carbonate identification in this area. To identify carbonates we therefore use the 2.5 μm band, though it can also be due to H_2O or OH in certain minerals (e.g., serpentines, chlorites, hydroxides, zeolites, sulfates). Based on observations of multiple spectra and analysis of the data set, the detection threshold for this band is set at 2.7% in band depth and a BDNR of 7.

In this study, carbonate compositions were not determined quantitatively based on 2.5 μm band position (as done e.g., in Beck, Beyssac, et al., 2024; Bishop et al., 2021), because spectral data at this wavelength with SuperCam is too uncertain and/or BDNR is generally not good enough in our data set for precise characterization of the position of the 2.5 μm.

2.5. Raman

The processing of the SuperCam Raman spectra was described elsewhere (e.g., Beyssac et al., 2023; Clavé et al., 2023; Lopez-Reyes et al., 2025).

2.5.1. Carbonate Detection and Characterization

Carbonates are characterized in Raman spectra by a series of internal vibrational modes of the CO_3^{2-} radical as well as lattice vibrations. With SuperCam, only the most intense of these modes has been detected in Martian targets so far: the C-O symmetric stretching mode of CO_3^{2-} (generally called ν_1), located between 1085 and 1095 cm^{-1} for most anhydrous carbonates. The position of the ν_1 mode within this range is primarily correlated with the composition of the carbonate (Beck, Beyssac, et al., 2024).

We first visually identify spectra with potential signal in the carbonate ν_1 range. We then fit the potential carbonate ν_1 peak with a Pseudo Voigt profile including a linear function for the local baseline. The signal-to-noise ratio (SNR) for each peak is computed by dividing the peak height by the standard deviation of the signal (after baseline subtraction) in a spectral range with no Raman signal (1300–1600 cm^{-1} range). Filters are then applied to the results of the fits: (a) signatures with a SNR lower than 3, or that appear too wide are excluded, as this is not consistent with a Raman carbonate mode; (b) for SNR values above 3, we confirm the detection of carbonate; (c) for signatures with a SNR above 12, we use the peak position from the fit to characterize the Mg# of the carbonate using the model from Beck, Beyssac, et al. (2024). For SNR values between 3 and 12, we find that the peaks are

Table 1
Summary of Criteria for Identification of Specific Minerals Based on LIBS, VISIR and Raman Data

	Parameters	Criterion	Conclusion
General	Images	Soil, tailings, floats	Exclude
		Bad focus	Exclude
LIBS	Distance	Distance > 6.5 m	Exclude
	O signal	SNR O $< m - 3\sigma$ (m: median, σ: std of distrib. of SNR O)	Exclude
	MOC	$SiO_2 \in [40; 50]$ wt.%	Coating: exclude
		$Al_2O_3 \in [7.0; 12.5]$ wt.%	
		$TiO_2 \in [0.6; 1.1]$ wt.%	
		FeOT $\in [10; 15]$ wt.%	
	SiO_2 and C/O	$SiO_2 \leq 30$ wt.%	Carbonate-bearing
		Normalized C/O >1.27 for 2 out of 3 considered C lines	
	MOC	$SiO_2 \geq 65$ wt.%	High silica
		$Al_2O_3 < 10$ wt.%	High silica
	Stoichiometric criteria	(details in Section 2.3.3)	Olivine
VISIR	Distance	Distance > 6.5 m	Exclude
	Illumination (in RMI)	Shadow	Exclude
	2.5 µm absorption	2.5 µm BD > 2.7%	Carbonate-bearing
		2.5 µm BDNR	Carbonate-bearing
Raman	Signal ν_1 CO_3^{2-}	SNR ≥ 3	Carbonate identified
		SNR ≥ 12	Carbonate with Mg#

Note. For VISIR, BD corresponds to the band depth and BDNR to the band depth to noise ratio.

too noisy to confidently constrain their positions and thus derive a reliable Mg#. Details on uncertainty computation are provided in the Text S3; Figures S10, S11; Table S3 of Supporting Information S1.

We sometimes use one spectrum per point and sometimes average all the spectra from a raster or a target together (specified each time). Averaging spectra can help increase the SNR for targets with relatively homogeneous carbonate content, but it provides an average carbonate composition and might thus hide some variability within a sample.

2.5.2. Detection of Olivine

Olivines are characterized in Raman spectra by a strong doublet around 820 and 845 cm^{-1}. The position of these modes is correlated to the composition of the olivine (Kuebler et al., 2006), however the signal is only good enough for such an analysis on a few of SuperCam's olivine detections along the traverse (Beyssac et al., 2023, 2026; Lopez-Reyes et al., 2025).

2.6. Data Set Selection Criteria

In this study, we use data acquired on bedrock with the SuperCam instrument up to sol 1282, covering the main units within Jezero Crater before the rover entered the Crater Rim. After selecting only bedrock targets, filtering out bad quality data and long distance targets and coatings as described above (criteria summarized in Table 1), we are left with ∼500 targets, whose distribution is detailed in Table S4 of Supporting Information S1.

3. Context – Mars 2020 Mission, Jezero Crater

3.1. Jezero Crater, Orbital Context and Carbonate Detections

3.1.1. The Regional Olivine-Rich Unit and Jezero Crater

From orbit, the Nili Fossae region in which Jezero Crater is located includes the most widespread (∼18,000 km^2) detection of olivine on Mars (Brown et al., 2010; Hamilton & Christensen, 2005; Hoefen et al., 2003; Mandon

et al., 2020). This regional olivine-bearing unit is a few tens of meter-thick and shows continuous internal banding that drapes the pre-existing topography. The primary lithology of this unit is locally altered, exhibiting locally some Fe-Mg-carbonates and Fe-Mg-phyllosilicates signatures (Ehlmann et al., 2008; Kremer et al., 2019; Mandon et al., 2020; Mustard et al., 2007). Proposed origins for this unit include: (a) igneous crustal rocks, such as shallow intrusions excavated by the Isidis impact (Hoefen et al., 2003); (b) lava flows (Hamilton & Christensen, 2005; Tornabene et al., 2008); (c) pyroclastic deposits (Bramble et al., 2017; Kremer et al., 2019; Rogers et al., 2018); (d) ejecta from Isidis impact forming event (Mustard et al., 2007; Palumbo & Head, 2017); (e) detrital sediments (Rogers et al., 2018). The Nili Fossae region also presents one of the strongest carbonate signatures observed from orbit on the surface of Mars (Carter et al., 2013, 2023; Ehlmann et al., 2008). Several authors showed that the carbonates in this region are associated with the olivine-rich unit, although only part of the regional unit appears carbonate-bearing based on orbital observations (Mandon et al., 2020).

Located in the Nili Fossae region, Jezero Crater is a ∼40-km-diameter impact crater with evidence of open-basin lake activity and signatures of aqueous alteration minerals (Goudge et al., 2012). Evidence of deltaic deposits, in particular in the Western Fan in Jezero Crater were documented from orbit (Goudge et al., 2017; Schon et al., 2012).

3.1.2. Carbonate-Bearing Formations Within Jezero Crater

Several carbonate-bearing formations were identified from orbit, using OMEGA and CRISM data. They were interpreted as being mostly Fe-Mg carbonates and distinguished in several, possibly distinct units based on geomorphological and mineralogical characteristics.

1. The light-toned floor unit was identified by Goudge et al. (2015) and characterized as the stratigraphically lowest unit in Jezero Crater, with signatures of olivine and carbonate from orbit. Proposed to be either a local expression of the regional olivine-carbonate unit, or a reworking of material from this regional olivine-carbonate unit, through aeolian or aqueous processes.
2. Carbonates were also identified in the sedimentary rocks of the Western delta and interpreted as likely detrital (Goudge et al., 2012, 2015, 2017), although the possibility of authigenic precipitation of carbonate cements was also considered (Goudge et al., 2017). Among the different facies characterized in the delta (Goudge et al., 2017, 2018), carbonates were identified in only a few locations, called curvilinear deposits and interpreted at the time to be point bar deposits of the topset distributary channels of the delta (meandering channels; Goudge et al., 2017; Horgan et al., 2020). Tarnas et al. (2021) then identified carbonates in a few more places in the Western Fan, namely the blocky, truncated curvilinear and undifferentiated smooth layers mapped on the Fan Top by Stack et al. (2020).
3. Thirdly, the Mottled Terrain (MT) was identified by Goudge et al. (2015) both inside and outside Jezero Crater; this unit is also characterized by strong olivine and carbonate signatures from orbit, possibly associated with another hydrated phase. Horgan et al. (2020) proposed that part of the MT might have a different origin from the rest, based on especially strong carbonate signature and specific location within a constrained range of altitude along the inner crater rim. They called this sub-unit Marginal carbonates (MC), and proposed that it might have been deposited on the shore of a lake among other possible interpretations. Following the distinction of the MC by Horgan et al. (2020), Tarnas et al. (2021) did not see any significant differences between the MC and the rest of the MT. Zastrow and Glotch (2021), however, observed a stronger contribution of Mg-rich carbonate in the MC than the rest of the MT and carbonate-bearing terrains within Jezero Crater.

3.2. Overview of the Mars2020 Mission, First 1282 Sols, and Previous Carbonate Detections

Between the landing of the Perseverance rover in Jezero Crater, in February 2021, and September 2024, its exploration was organized into four scientific campaigns: Crater Floor (sols 0–421; Sun et al., 2023), Fan Front (sols 422–710; Williams et al., 2023), Upper Fan (sols 711–909; Nachon et al., 2024) and Margin Unit (sols 910–1251; Horgan, Garczynski, Barnes, et al., 2024; Horgan, Garczynski, Gupta, et al., 2024). The 31 km of traverse up to sol 1282, main units and members are illustrated in Figure 1. Note that the chronological order of exploration (represented in Figure 1d) does not always enable to easily represent unit boundaries, when the rover goes back and forth between units. For example, the Rockytop member was investigated in the middle of the Fan Front campaign although it belongs to the Upper Fan. The details of sol limits for each unit/sub-unit are

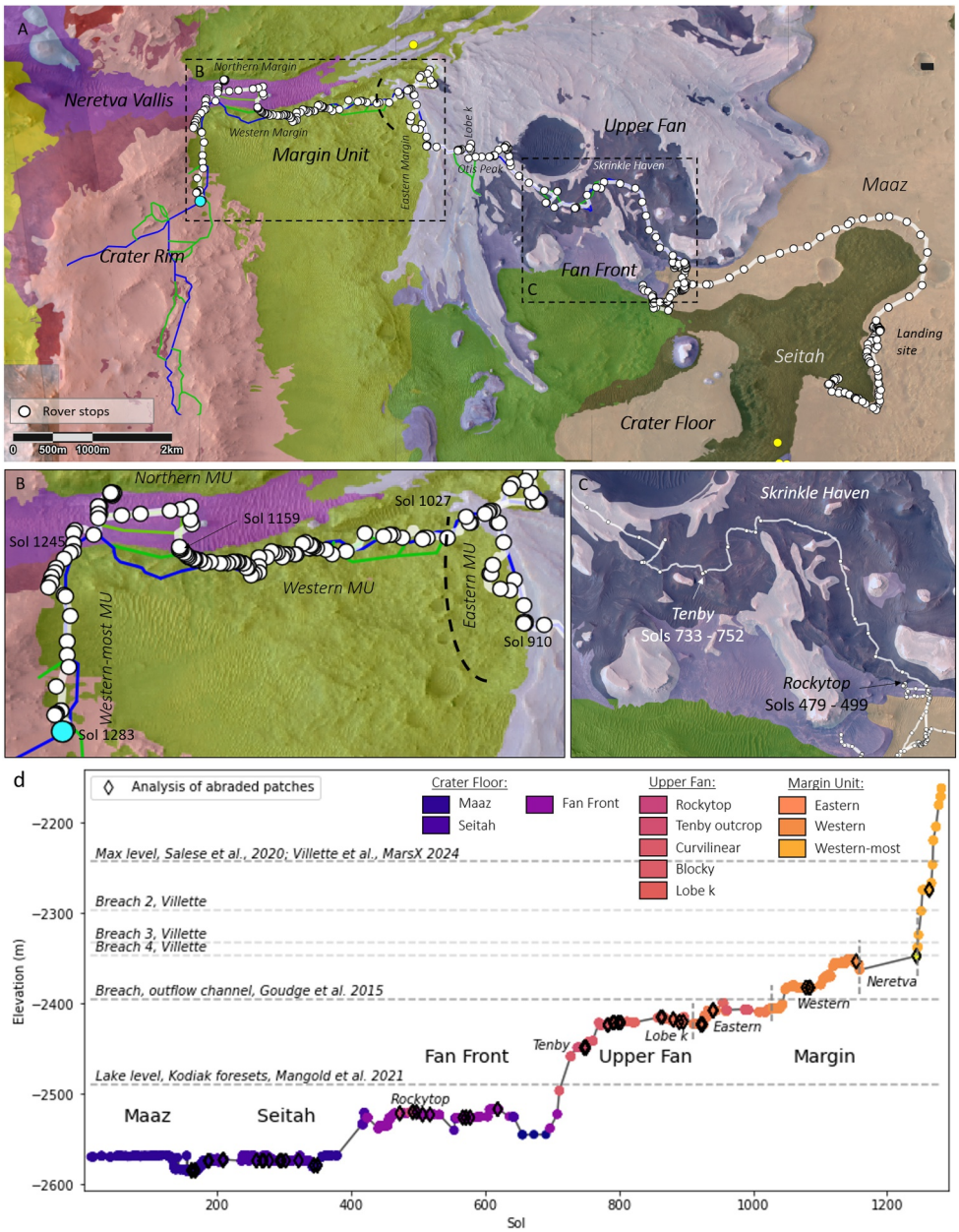

Figure 1. Overview of the traverse of the rover over the first 1282 sols of the Mars 2020 mission. (a) Overview of the traverse on the geological map (Stack et al., 2020): (b, c) Close ups on part of the Upper Fan and Margin Unit; (d) Elevation of SuperCam targets along the traverse compared to documented levels of the paleolake in Jezero Crater (Goudge et al., 2015; Mangold et al., 2021; Salese et al., 2020; Villette et al., 2024). The color code corresponds to sub-units, the sol limits being summarized in Table S5 of Supporting Information S1. Abraded patches are shown with black diamonds.

summarized in Table S5 in Supporting Information S1. Correspondences between orbital and in situ terminologies for different units are summarized in Table 2.

3.2.1. Crater Floor Campaign

During the Crater Floor Campaign, the rover explored two distinct formations, corresponding to the Mafic Floor and the Light-toned floor described by Goudge et al. (2012).

The stratigraphically lower one is Séítah, an expression of the light-toned floor unit. Based on the in situ characterization with the scientific payload of Perseverance, it was interpreted to be a weakly altered olivine-cumulate

Table 2
Different Units and Members Explored by the Perseverance Rover and Relationship to Units and Members Identified and Mapped From Orbit

	M2020 name	Stack et al., 2020—Remapping	Units/members identified from orbit
Crater Floor	Máaz	Crater floor fractured rough	Mafic Floor (Goudge et al., 2015)
	Séítah	Crater floor fractured 1	Light-toned floor (ltf) (Goudge et al., 2015)
Fan (Western)	Fan Front	Delta thinly layered	
	Skrinkle Haven	Delta truncated curvilinear layer	(Point bar deposits)
	Otis Peak	Delta Blocky	
			Mottled Terrain (MT) (Goudge et al., 2015)
	Margin Unit	Margin fractured	Marginal Carbonates (Horgan et al., 2020)

(Beyssac et al., 2023; Farley et al., 2022; Liu et al., 2022; Mandon et al., 2023; Scheller et al., 2022; Tice et al., 2022; Wiens et al., 2022). In particular, some Fe-Mg carbonates were identified in situ in Séítah and interpreted to result from in situ, isochemical alteration of the mafic rocks of Séítah (Clavé et al., 2023; Corpolongo et al., 2023; Scheller et al., 2022; Tice et al., 2022).

Stratigraphically above Séítah, lies the Máaz formation, corresponding to Goudge's Mafic Floor and which was interpreted to have formed through successive lava flows (Farley et al., 2022; Horgan et al., 2023; Udry et al., 2023; Wiens et al., 2022). Máaz also shows indications of weak alteration and late fluid circulation, in the form of sulfate and perchlorate salts, in particular (Mandon et al., 2023; Meslin and SuperCam Team, 2022; Tice et al., 2022; Wiens et al., 2022).

3.2.2. Exploration of the Western Fan

Long distance images acquired by Perseverance within the first months of the Mars 2020 mission confirmed the deltaic nature of the sedimentary deposits of the Western Fan (Mangold et al., 2021). These rocks were then investigated in situ by Perseverance during the second and third scientific campaigns of the mission, dedicated to the Fan Front and Upper Fan, respectively. We consider separately the Fan Front (Shenandoah formation), which stratigraphy was described in detail in Stack et al. (2024), and the Upper Fan, which is divided into the Tenby formation and the Otis Peak formation.

The Shenandoah formation represents the base of the fan with a predominance of recessive layers composed of medium to coarse sandstones, with fine sandstone to siltstone in the Hogwallow Flats member (Stack et al., 2024). Strata are subhorizontal with thicknesses of several cm to tens of cm. This formation remains geometrically uniform over several km at the base of the fan.

The Tenby formation comprises the Shrinkle Haven member at the base, starting at the Rockytop outcrop (Gupta et al., 2024; Ives et al., 2005; Stack et al., 2024). To better investigate the variability in this Shrinkle Haven member, we distinguish the Tenby outcrop (sols 733–752) from the rest of the Skrinkle Haven member, as it was a location with a large number of targets. For the uppermost Otis peak fm (Gwizd et al., 2024), we also split the Lobe k (sols 871–897) from the rest of the Otis Peak formation, as it is a geographically distinct location corresponding to a distinct delta lobe (Kronyak et al., 2023).

At the base of the Tenby formation, the Rockytop outcrop displays conglomerates with subrounded granules and small pebbles dipping gently toward south (Figures 2a and 2b). At the Tenby outcrop, 60 m higher in elevation in the Upper Fan, strata dip up to 35° (Gupta et al., 2024) while the texture is dominated by coarse sandstones with local pebbles (Figures 2c and 2d). This formation is dominated by sediments interpreted to have been deposited subaqueously by gravitational sliding. Locally, a smooth, dark gray blanket covers the rock texture (Figure 2d; Garczynski, Horgan, et al., 2025). It is interpreted as a fracture fill or coating from a post-depositional stage, and was analyzed in a couple of locations. In contrast to the Shenandoah formation, it also displays large variability in geometry of bedsets, including a variability in dip orientation, although southern dips remain predominant (Mangold et al., 2023). Where analyzed, sedimentary rocks are also well-cemented and more resistant than the Shenandoah formation (Gwizd et al., 2024). In contrast, the Otis Peak formation, higher on the Upper Fan, displays strata with subhorizontal dip and generally coarser texture from sandstones to boulder conglomerates

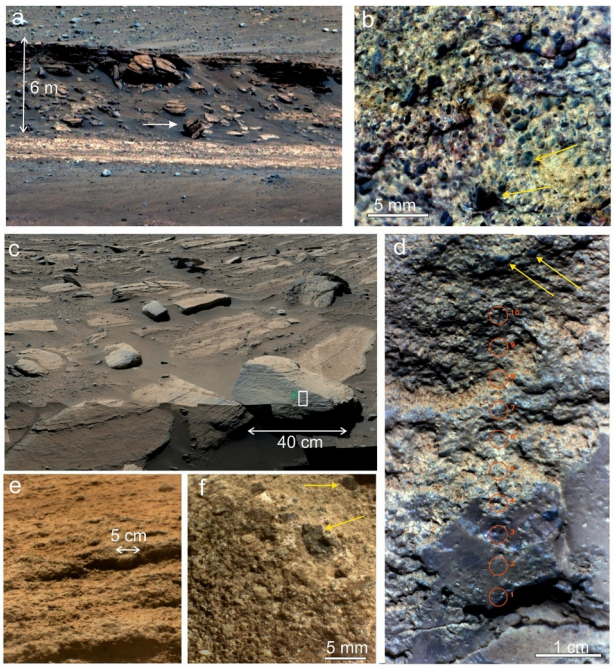

Figure 2. Representative outcrops of the Jezero western delta in which carbonates have been detected. (a) Mastcam-Z image of the base of the delta with the Rockytop outcrop within the 6 m high scarp (sol 429, zcam08452) located at the base of the Tenby formation immediately overlying the Hogwallow Flats light-toned deposits. The white arrow indicates the fallen block where the SuperCam target *Fourway* has been analyzed. (b) Close-up on the SuperCam target Fourway (sol 407, scam01407, Gaussian stretch). The texture is that of a coarse sandstone to granule-conglomerate containing rounded, subrounded and subangular grains. (c) Mastcam-Z mosaic (sol 743, zcam08747) of Tenby outcrop, which is part of the Tenby formation. The white box indicates the location of detail (d). (d) SuperCam RMI of the *Crymych* target (sol 745, seq04745, gaussian stretch). The Tenby outcrop displays coarse sandstones with local granules and pebbles exposed in steeply dipping beds. Red circles represent fields-of-view of infrared spectrometer observations. (e) Outcrop Onahu (sol 781, scam01781) in the Otis Peak formation, overlying the Tenby formation. The strongly weathered outcrop of this formation is composed of pebbly sandstones and conglomerates (5 cm pebble with a white arrow). (f) Target *Ouzel_Falls* (sol 791, scam01791) located nearby Onahu displaying several mm large clasts with various degrees of rounding. Yellow arrows indicate some of the local most visible rounded or subrounded mm-size granules.

(Gwizd et al., 2024), with a varying degree of clast rounding from subangular to rounded (Figures 2e and 2f). The overall sequence is interpreted as deltaic-dominated sedimentary rocks with early fluvial deposits and lakebeds at Shenandoah, deltaic foresets and toesets in Tenby formation (Figures 2a–2d) and fluvial deposits (mostly topsets) in Otis Peak fm (Mangold et al., 2023; Figures 2e and 2f). The Shenandoah formation does not show any primary mineralogy and is dominated by sulfates and clays minerals while the Tenby and Otis Peak formations exhibit olivine and carbonates (Dehouck et al., 2024).

3.2.3. The Margin Unit

The exploration of the orbitally identified Marginal Carbonates was the objective of the fourth scientific campaign of the Mars 2020 mission; in this context the unit was named Margin Unit (Figure 1). Based on several, independent lines of evidence (surface structure, microtexture, chemistry, also presented in Williford et al. (2026), we distinguish the Eastern and Western parts of the Margin Unit. We separate the two parts at sol 1027 based first on an observed change of carbonate chemistry. Perseverance left typical Margin Unit rocks to explore the Neretva Vallis channel between sols 1160 and 1245 (Hurowitz et al., 2025). After crossing this channel, Perseverance encountered rocks corresponding to the Margin Unit on the Northern side of the channel (sols 1205–1212) that were, however, excluded from this study due to their spatial separation from the main MU and insufficient data to verify that the same processes have occurred there. After investigating the channel, the rover explored the Western-most part of the Margin Unit as seen from orbit, along the inner rim of the crater (from sol 1245; Figure 1). Although the Margin Unit Campaign officially ended on sol 1251, bedrock of similar characteristics were observed without interruption up to sol 1282, and these are therefore included in this study.

The Margin Unit (MU) is located west of the sedimentary deposits of the delta, at elevations similar to the Fan Top and higher (Figure 1). This unit is older than the deltaic deposits as observed from local stratigraphic contacts (Hamran et al., 2024). The different sub-unit identified within the Margin Unit present slight differences in texture. The Eastern MU presents planar, cm-thick beds generally showing up as flat, paver-like surfaces, and locally weathered in circular features (Figures 3a and 3b). The texture is granular with mm-size, subangular to subrounded grains. Despite the layered aspect of the Eastern MU, none of the layers observed displays any obvious sign of bedforms (cross-bedding, channel shapes, etc.), or alternatively viscous patterns typical of lava flows. The Western MU displays a more massive texture with high-standing blocks (Figures 3c and 3d), although a bedding is still visible locally. The texture is also composed of mm-size grains but with predominant angular shapes. The Western-most MU is located further West and South and some of it was not necessarily always mapped from orbit as part of this unit. However, it's laterally continuous with the rest of the Margin Unit and the texture and composition fits clearly the MU characteristics (Figures 3e and 3f). There, outcrops vary from pavers to high-standing outcrops and the texture is granular, again, with relatively angular or subangular, 1-2 mm-size grains.

4. Results

4.1. Chemistry and Mineralogy Along the Traverse

4.1.1. With LIBS

Using the MOC, we can observe general trends and variations in composition along the rover traverse, as the rover explored different units (Figure 4 and Figures S12–S14 in Supporting Information S1).

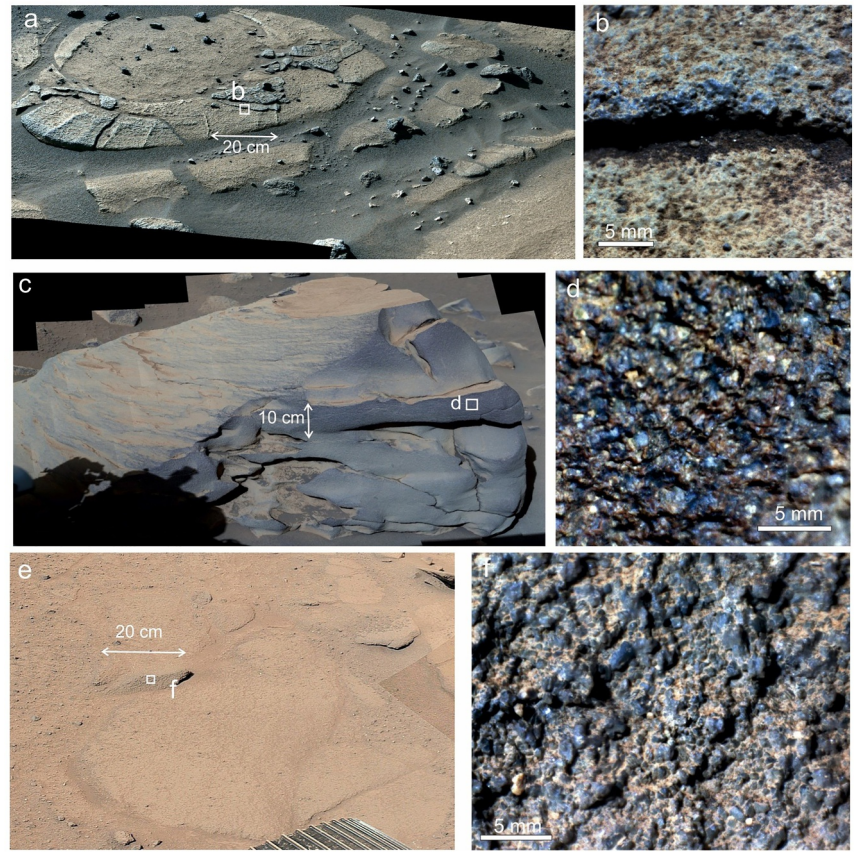

Figure 3. Outcrops of the Eastern Margin Unit (a, b), Western Margin Unit (c, d) and Westernmost Margin Unit (e, f). (a) Mastcam-Z mosaic next to the Hans Amundsen memorial site (sol925, seq08932) showing a concentric weathering pattern on layered rocks. (b) The texture at RMI scale of the target *Drysdale* (sol 926, seq02926, gaussian stretch) is granular with mm-size subangular to subrounded grains strongly packed together. (c) Mastcam-Z mosaic (sol 1069, zcam04745) of Bunsen Peak outcrop displays a massive texture. (d) The SuperCam RMI of the *Rainbow_Lake* target on the Bunsen Peak outcrop (sol 1069, scam01069, gaussian stretch) show a rough texture at cm-scale with mm-size angular grains. (e) Navcam image (sol 1270) of paver rocks with a small ledge of fresh outcrop on which the target SuperCam *Tanner_Graben* has been taken (sol 1271, scam01271, Gaussian stretch). (f) *Tanner_Graben* is composed of angular to subangular grains of 1–3 mm in diameter.

Looking at the distribution of the major elements in all bedrock targets (gray violins in Figure 4), we observe that the composition is overall dominated by silicates, with SiO_2 mostly between 30 wt.% and 65 wt.%. However, in the Upper Fan and even more so in the Margin Unit, we observe an increased number of points with either low or high SiO_2 content (<30 wt.% and >65 wt.% SiO_2, respectively). Al_2O_3 stays at low values (typically less than 5 wt.% Al_2O_3) in Séítah, the Fan Front and the Margin Unit, whereas higher values were detected in Máaz and the Fan Front. We observe important variations in FeO and MgO contents along the traverse, and within each unit, with for example, FeO abundances going almost from 0 to 55 wt.% in the Upper Fan and MgO averages going from around 5 wt.% in Maaz to almost 25 wt.% in the Margin Unit. Distributions of CaO and Na_2O are included in the Supporting Information (Figure S13 in Supporting Information S1). Overall, CaO is locally enriched in small Ca-sulfate veins visible all along the traverse, though with variable density and especially present in the Fan Front (Nachon et al., 2023). In bedrock, CaO is highest in Máaz and the Fan Front and stays around 5 wt.% or lower in other units. Na_2O is generally rather low (~2 wt.% or lower), although some higher values were measured in Máaz (~3–4 wt.%).

In Figure 4, we also observe that the carbonate-bearing points (colored violins) are generally rich in FeO and MgO (covering the higher range of bedrock compositions in most units). Observed carbonate-bearing points are depleted in Al_2O_3, CaO and Na_2O compared to the bulk chemistry (Figure 4 and Figure S13 in Supporting

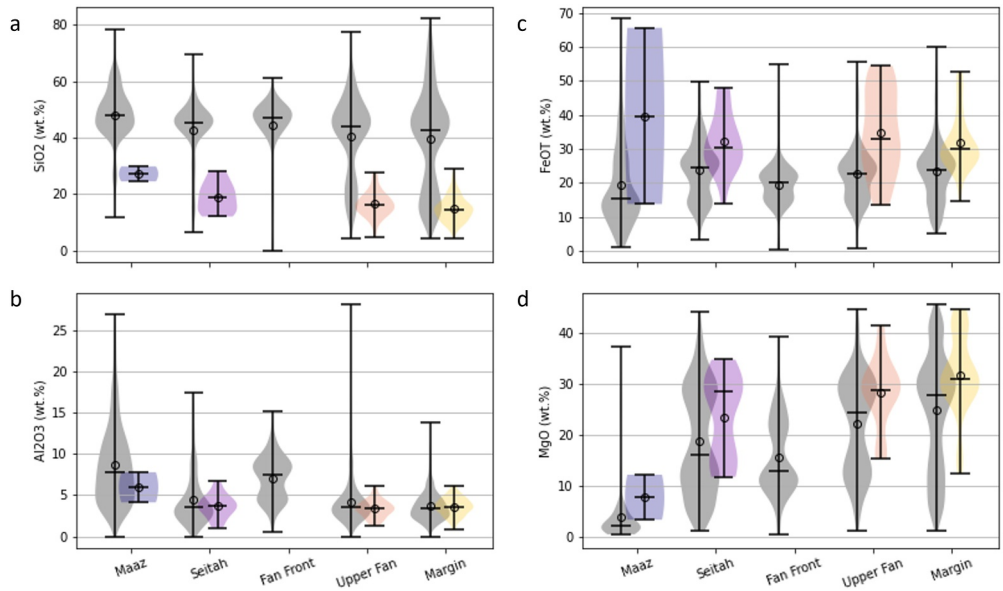

Figure 4. Compositions of main units analyzed with SuperCam based on MOC. The distribution of MOC values for SiO_2 (a), Al_2O_3 (b), FeOT (c) and MgO (d) for bedrock targets in each unit is shown in gray; the composition of carbonate-bearing points in each major unit is in color (color-coded to unit, same as in Figure 1; no carbonate-bearing point was identified in bedrock in the Fan Front, hence the absence of a colored violin for this unit). Median values are indicated with a dash, means with a circle.

Information S1). We therefore consider that the carbonates in these rocks belong to the siderite-magnesite solid-solution and we call them Fe-Mg carbonates in the following.

Considering that Séítah represents a relatively weakly altered, previously well-characterized igneous unit with mafic to ultramafic composition, we use it as a reference to compare the composition of other mafic/ultramafic units encountered later in the traverse, that is, the Upper Fan and Margin Unit. We compare the bulk compositions (median values) of the different units to the bulk composition of the Séítah formation (Figure 5a), and we observe a similarity between the Upper Fan and Margin Unit, which are both close to the composition of Séítah, consistent with mafic to ultramafic compositions. Some subtle differences are observed between these units, with an increasing MgO content and overall decreasing TiO_2 and CaO contents along the traverse, but these units appear to be in family, with compositions dominated by SiO_2, FeO and MgO, and relatively low Al_2O_3, TiO_2, CaO, Na_2O and K_2O. The range of SiO_2 contents is wider in the Margin Unit than in Séítah, consistent with Figure 4. The Máaz unit and the Fan Front appear distinct from this first group of units, with relatively low MgO contents (especially in Máaz), and relative enrichments in Al_2O_3 and TiO_2, as well CaO and Na_2O for Máaz especially.

Within the Margin Unit, we note an increase of MgO content and decrease of CaO content from East to West (Figure 5b). Moreover, the range of SiO_2 content in the Western-most Margin Unit data is significantly narrower than in the Eastern and Western areas, with few high or low SiO_2 points.

Using Spectral Unmixing scores, we compared the distribution of certain minor elements of interest along the traverse (ex. Cr, S, Mn, …, listed in Section 2.3.4). Although we observe some variability, with local enhancement of these elements, the carbonate-bearing points are generally not particularly enriched in any of these elements. Of note are points elevated in Ti and Cr, interpreted as possible chromite or Cr-rich ulvöspinel grains (consistent with Beyssac et al., 2023, 2026). These were observed regularly in all olivine-rich units along the traverse (Figure S14 in Supporting Information S1) and contribute to the large standard deviation of the TiO_2 abundances visible in Figure 5. Sulfur enrichments in LIBS are also observed locally, always associated with high CaO content, and visible pore/fracture filling in RMI images, interpreted as Ca-sulfate (presented in Schröder et al., 2024).

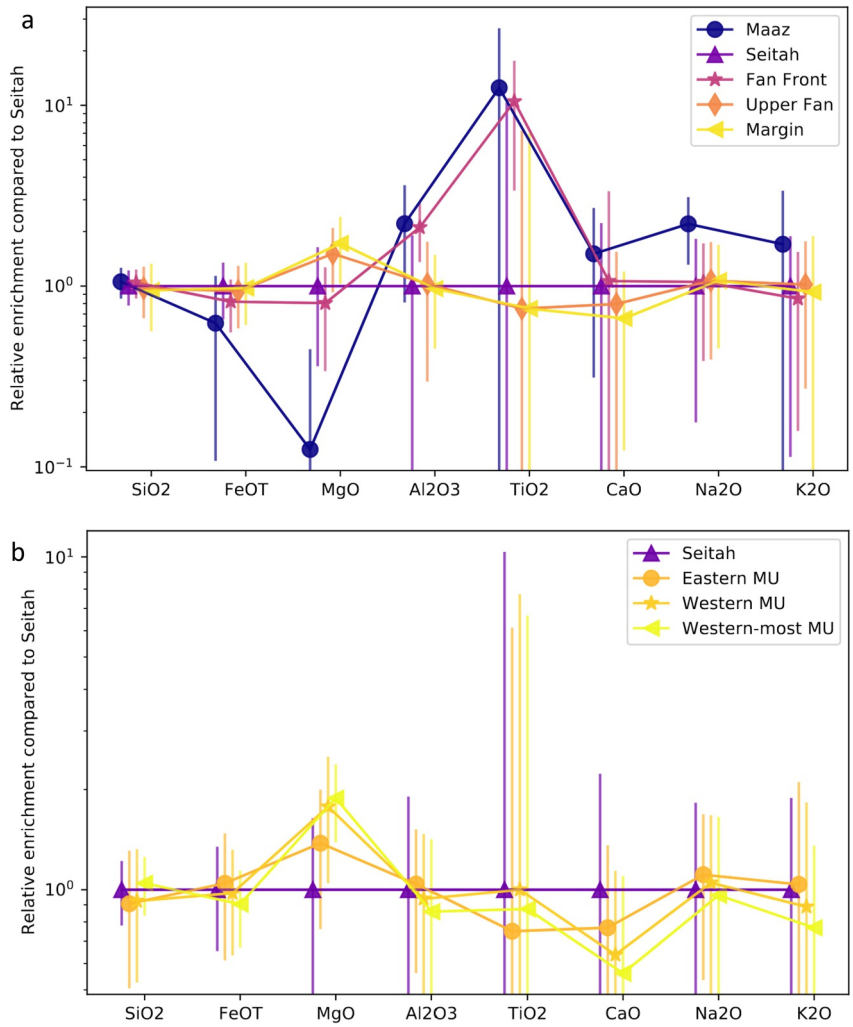

Figure 5. Median compositions of bedrock in different units compared to the median composition of Séítah based on the MOC. Error bars show the standard deviation of the distribution observed in each unit for each element. (a) Unit-scale; (b) Sub-unit scale, within the Margin Unit.

4.1.2. With Raman

With Raman spectroscopy, carbonate and olivine were both detected in Séítah, the Upper Fan and the Margin Unit, and not in Máaz or the Fan Front. Examples of carbonate- and olivine-bearing spectra from these three units are shown in Figure 6; more spectra are shown in Figure S15 of Supporting Information S1.

Carbonates were detected in multiple locations along the traverse and we saw an increase in number of detections as well as quality (overall SNR) of the detections along the traverse from Séítah, through the Upper Fan, to the Margin Unit (Figure 7a). Looking into the Mg# derived for the carbonate detections with sufficient SNR (Figure 7b), we observe a significant variability in carbonate Mg# within the Upper Fan and the Margin Unit both, from around 30 (Tenby area around sol 750) to around 70 (Otis Peak formation, especially around sol 800 and Western Margin around sols 1050–1080).

4.1.3. With VISIR

As illustrated in Figure 8, the VISIR data in Séítah, the Upper Fan and the Margin Unit show variable contributions of:

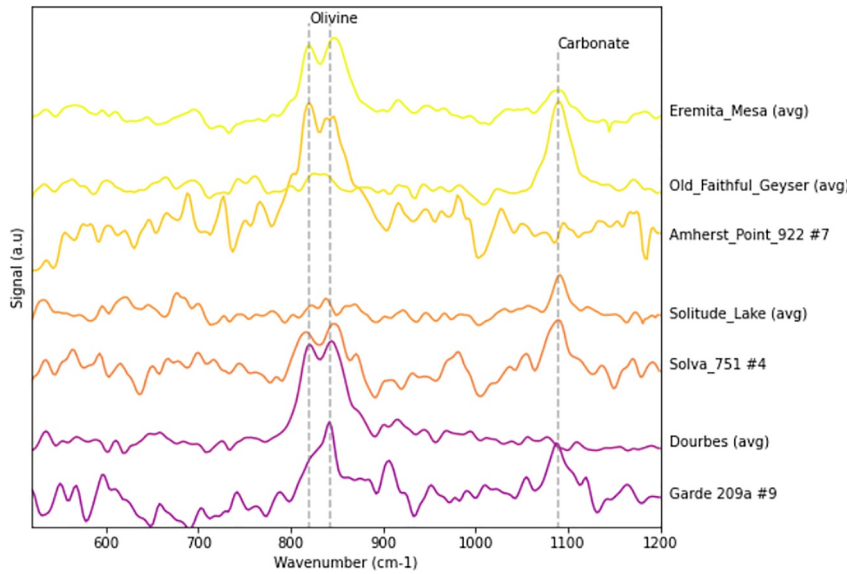

Figure 6. Carbonate- and olivine-bearing Raman spectra observed in Séítah (*Garde* and *Dourbes*; purple spectra), the Upper Fan (*Solva* and *Solitude_Lake*; orange spectra) and the Margin Unit (Eastern: *Amherst_Point*, Western: *Old_Faithful_Geyser* and Western-most: *Eremita_Mesa*; light orange to yellow spectra). The dashed lines indicate reference peak position for olivine (820 and 842 cm^{-1}) and Fe-Mg carbonate (1089 cm^{-1}). Spectra were normalized and the contribution of the optical fiber subtracted; they are represented with an offset for better visibility. When "avg" is indicated after the target name, the presented spectrum is an average of all the Raman spectra collected on the target; otherwise, the number of the point where the spectrum was collected is indicated with a #.

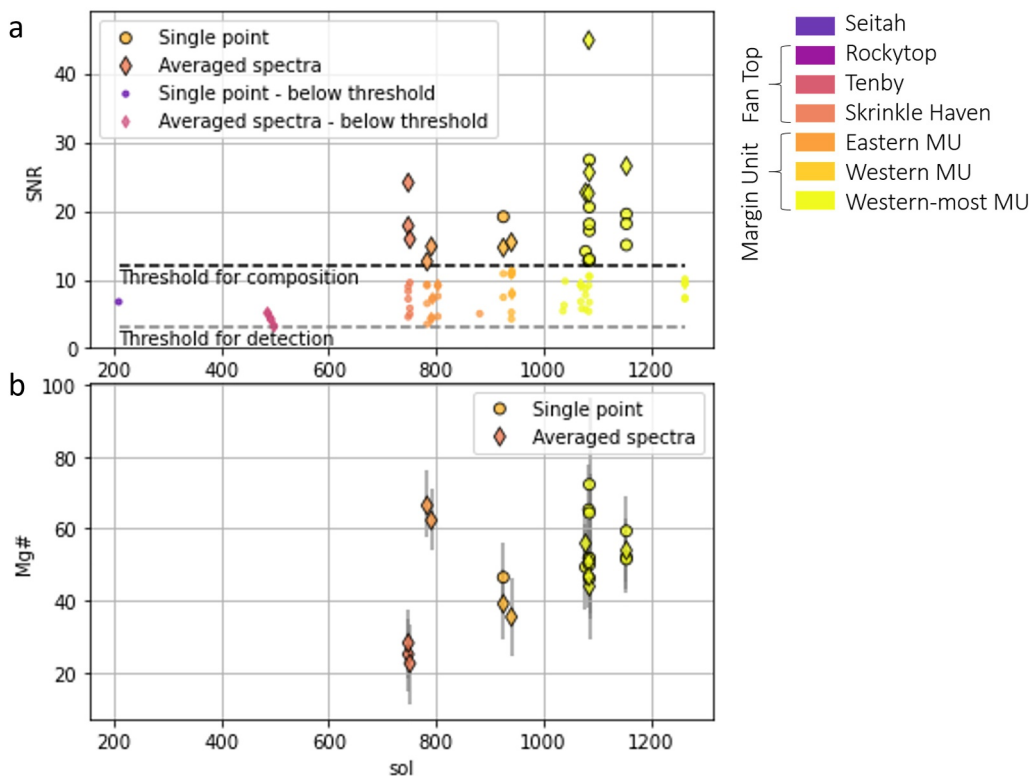

Figure 7. SNR of carbonate ν_1 mode in Raman spectra (a), and corresponding Mg# for detections above the composition characterization threshold (b) along the traverse (sol number). Markers are color coded to location along the traverse, including values derived from single point spectra (dots) and averages of one or more rasters (diamonds).

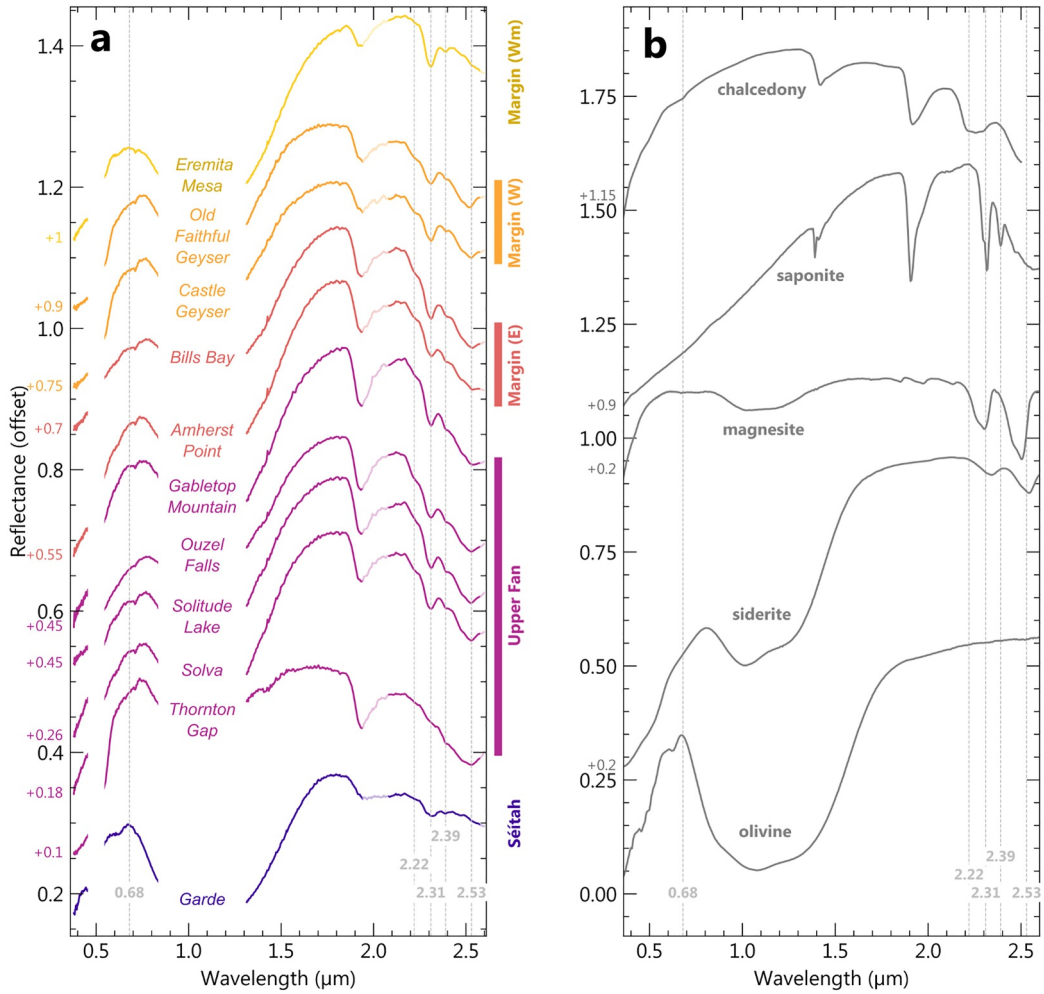

Figure 8. (a) Average spectra of olivine- and/or carbonate-bearing abraded patches. *Garde* was chosen as an example of Séítah spectrum; all abraded patches analyzed in the Upper Fan and Margin Unit are shown. "Dips" at ∼0.62 and ∼0.71 μm are artifacts from where VIS detector regions join. (b) Laboratory reference spectra for relevant minerals (Relab spectra ID: olivine C1PO47; siderite CACB08 (0–45 μm); magnesite CACB06 (0–45 μm); saponite C1SA53; USGS specimen ID: chalcedony CU91-6A). The Mars spectra all look in family, with variable contributions of olivine, carbonate (such as magnesite and siderite) and phyllosilicates (such as saponite) and silica (e.g., chalcedony).

1. A broad absorption band centered around 1 μm (center of the band not visible with SuperCam but both sides of the slopes are in VIS and IR spectral ranges respectively) attributed to Fe^{2+} in either olivine or carbonate. The position of the left shoulder of this band can be interpreted in terms of alteration of the olivine: most pristine olivine spectra have reflectance peaks in the visible centered shortward of 0.7 μm, while Fe-bearing carbonates most often have it centered longward of 0.7 μm (Lapo et al., 2024). The position of this peak at 0.68 μm for Séítah and the Western-most Margin abraded patches reflects the greater influence of pristine olivine in these two areas.
2. A strong 1.9 μm absorption due to H_2O;
3. A weak absorption band centered at 2.22 μm, either caused by Al-OH or Si-OH. Considering the high-Si points detected by LIBS and the overall low Al content, this band is attributed to Si-OH.
4. Pair of absorptions at near 2.3 and 2.5 μm attributed mainly to carbonates;
5. A weak absorption band centered at 2.39 μm is visible in most of these spectra; it is attributed to phyllosilicates, which likely also contribute to the 1.9 μm hydration band. Moreover, in some spectra (e.g., *Amherst_Point*), the 2.3 micron band is significantly deeper and narrower compared to the 2.5 μm band for what is expected for pure carbonate, which may be the contribution of phyllosilicates on top of some (weaker) carbonate signature, consistent with the presence of the small 2.39 μm band.

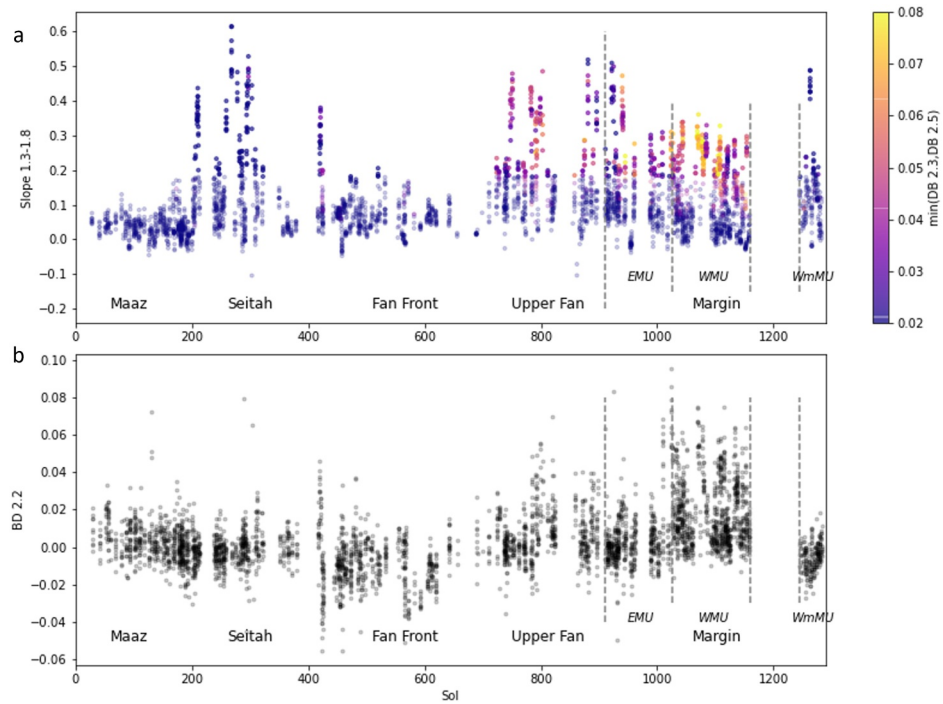

Figure 9. VISIR spectral parameters along the traverse. (a) Fe^{2+} spectral parameter (slope between 1.35 and 1.8 μm) as a function of sol, color coded to carbonate spectral parameter (minimum of 2.32 and 2.53 μm band depths). Deep Fe^{2+} absorptions, correspond to either olivine or carbonate; when the corresponding points have strong 2.32 and 2.53 μm bands, it is likely related in large parts to carbonates. (b) 2.2 μm band depth parameter, corresponding mostly to Si-OH (confirmed by LIBS) along the traverse as a function of sol.

The spectra of the rocks abraded in the different geological formations within the crater illustrated in Figure 8 are all in family, and they are representative of the surrounding bedrock. The most distinct spectra are: (a) *Garde*: Séítah is generally less altered with weaker hydration, hydrater/hydroxylated silica, carbonate and phyllosilicate signatures and a more pristine olivine signature; (b) *Thornton_Gap*: the Rockytop area at the base of the Upper Fan is distinct with a significant sulfate contribution (discussed later); (c) the lack of silica and carbonate signatures in *Eremita_Mesa*, in the Western-most MU is noticeable compared to the rest of the MU; the spectrum is dominated by more pristine olivine and phyllosilicate signatures.

Looking at bedrock targets along the entire traverse (Figure 9a), we observe a strong influence of the Fe^{2+}-absorption band—manifested by the 1.3–1.8 μm slope—in Séítah, the Upper Fan and the Margin Unit, attributed to olivine and/or carbonate. In Séítah, this is accompanied by only weak absorptions at 2.32 and 2.53 μm (blue color), indicating overall weak contributions from alteration minerals, with an Mg-OH-bearing phase being the prime alteration phase detected (Mandon et al., 2023). In the Upper Fan, Eastern and Western MU, the Fe^{2+} absorption band is accompanied by very strong carbonate signatures—especially in the Western MU (yellow), indicating an increase of carbonate abundance and/or their grain size. In the Western-most MU, significant Fe^{2+} absorption bands are observed again, but the associated carbonate signature is weak (blue color), indicating lower carbonation than in the rest of the MU. The distribution of 2.2 μm absorption along the traverse is similar to that of carbonate (Figure 9b): points with a significant 2.2 μm band are detected mostly in the Upper Fan and Western Margin Unit, and the relatively high SiO_2 and low Al_2O_3 contents observed in LIBS enable the identification of this band as mostly Si-OH rather than Al-OH. Very few Si-OH absorptions were observed in the Western-most MU, indicating low silica abundance in that area. These observations of natural rock surfaces are all consistent with the observations made on the spectra of abraded patches along the traverse.

4.1.4. Distribution of Mineral Detections

As shown above, LIBS, Raman and VISIR data consistently reveal the presence of olivine and carbonates in Séítah, the Upper Fan and the Margin Unit; additionally, with LIBS and VISIR spectroscopy, hydrated/

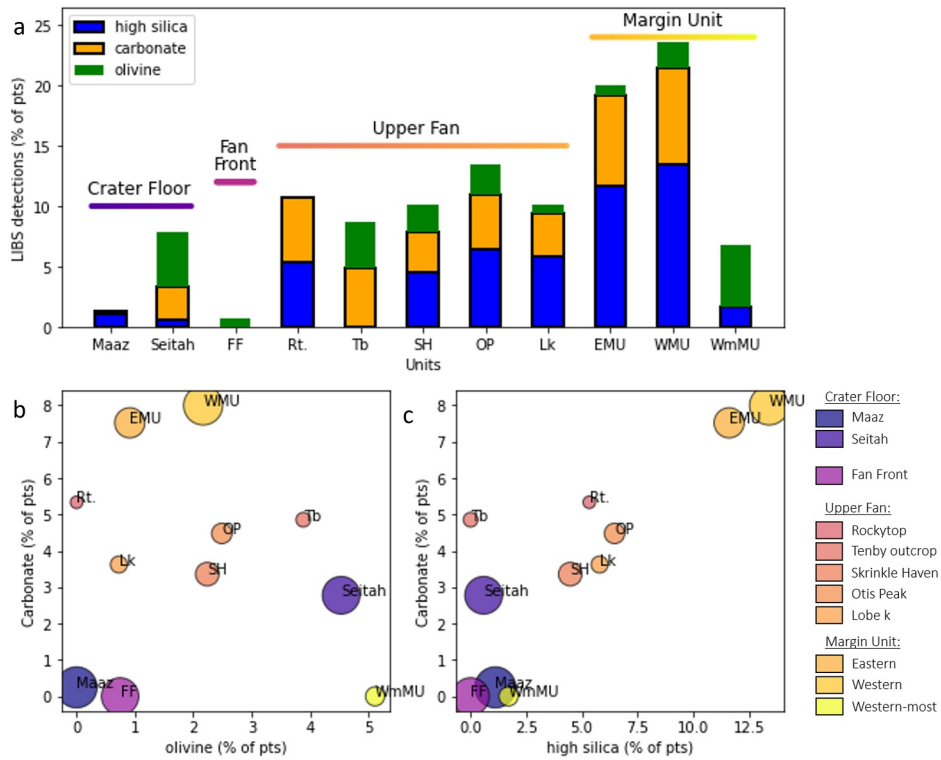

Figure 10. LIBS detections of olivine, carbonate and silica in bedrock along the traverse (criteria listed in Table 1). (a) Stacked bar chart with number of detections per mineral per unit/sub-unit. Secondary minerals are indicated by data shown with a thick black outline; primary minerals (olivine) with no outline. (b, c) Number of carbonate detections as a function of the number of detections of olivine (b) and high silica (c) per unit/sub-unit. The size of the markers is based on the number of observations included per sub-unit (min: 75 points in Rockytop; max: around 800 points in Máaz). The labels and colors correspond to the sub-units: FF for Fan Front, Rt for Rockytop, Tb for the Tenby outcrop, SH for Skrinkle Haven, OP for Otis Peak, Lk for Lobe k, and EMU, WMU and WmMU for Eastern, Western and Western-most Margin Unit, respectively.

hydroxylated silica is detected in these same units. Although we do not detail it here, low calcium pyroxene was also detected with LIBS, in association with olivine along the traverse (Beyssac et al., 2026).

To first order, the distribution of minerals along the traverse can be characterized using their frequency of detection. This is shown in Figure 10 for LIBS. A multi-technique comparison is included in the Supporting Information (Figure S16 in Supporting Information S1), but the low number of points (Table S5 in Supporting Information S1) and changes of textures along the traverse prevent going to the sub-unit level with Raman and VISIR data.

Máaz and the Fan Front are olivine-, carbonate- and silica-poor, so we do not comment on them further. Focusing on Séítah, the Upper Fan and the Margin Unit, we note overall a decrease of olivine abundance, accompanied by an increase of carbonate and silica from Séítah to the Upper Fan, to the Margin Unit (Figure 10). This is in agreement with independent observations with VISIR and Raman spectroscopy (Figure S14 in Supporting Information S1). Moreover, in the scatter plot we observe a correlation of the number of carbonate and silica detections in most olivine-rich areas (Figure 10). The main exceptions are: Rockytop (Rt.) where we do not see olivine; the Tenby outcrop (Tb.) which lacks silica; the Western-most MU (WmMU), which is olivine-rich but carbonate-poor (although carbonate was still detected with Raman in that area, in the *Eremita_Mesa* patch, in particular).

While we cannot derive mineral abundances at the point level from our observations, we can propose estimates for bulk carbonate abundance in the following way. We use a parameter L_c called the critical level, which is the threshold abundance with 5% or less of false positives. In other words, at least 95% of points whose measured abundance is above L_c are carbonate-bearing. For carbonate identification with one-point LIBS measurements in

Table 3
Some Quantitative Constraints on the Abundance of Carbonate in Bulk Rocks Based on LIBS Results

	Lower limit of carbonate content (wt. %)	Possible carbonate-bearing points (%)	Estimated approximate carbonate content (wt. %)
Séítah	1.4	12.4	1–5
Upper Fan	2.1	23.6	3–9
Eastern MU	3.9	39.6	6–16
Western MU	4.1	32.3	5–13
Western-most MU	0.0	8.5	1–3

Note. 1st column: Very conservative lower limit of carbonate content in bulk rocks of different units and sub-units along the traverse, based on number of detections of carbonate-bearing points with LIBS. *2nd column:* Percentage of LIBS points with a SiO_2 content below 30 wt.% and CaO below 8 wt.%, that likely contain some carbonate. *3rd column:* Estimated approximate carbonate abundance assuming a range of carbonate content in carbonate-bearing points of 55–95 wt.% and that possible carbonate-bearing points (low SiO_2, low CaO, C/O not elevated enough) could contain 5-35 wt.% carbonate.

Martian atmosphere, Beck, Meslin, et al. (2024) characterized a L_c as 6.85 wt.% carbon. To go from carbon elemental abundance to the abundance of carbonate mineral, we use an average carbonate composition of Mg# 60 (see Section 4.1.5). For this composition, the carbon content in a pure Fe-Mg carbonate is 12.4 wt.% C. The critical level L_c is thus around 55 wt.% carbonate mineral abundance (more details in Table S7 of Supporting Information S1). Based on the number of detections per unit and this parameter, we propose different estimates and ranges of carbonate abundance. First, we can derive lower limits for carbonate abundances using this L_c, and assuming that the large number of SuperCam LIBS analyses, and kilometers of traverse they sample, enable to extrapolate the bulk composition of a unit. This is supported by the detections of carbonates all along the traverse, as shown in Figures 7 and 9. In the bulk Margin Unit, around 7% of points were identified as carbonate-bearing. Based on the definition of the critical level L_c, at least 95% of these 7% contain L_c = 55 wt.% (or more) carbonate mineral. We can thus give a lower limit for the carbonate content in the Margin Unit of at least 3.6 wt.% carbonate ($0.95 \times 0.07 \times 55$ wt.% CO_3). This number is a lower limit of the true carbonate content since (a) points with carbonate content under 55 wt.% may remain undetected; and (b) the carbonate content in some of the points we identified as carbonate-bearing is likely significantly higher than 55 wt.%. Second, we can in part address this first limit: we consider that all points with SiO_2 abundance below 30 wt.% must contain some non-silicate phase. Only chromites, Ca-sulfate and Fe-Mg-carbonates were detected in significant amounts in the Margin Unit. Chromites were found as grains so small, mixed with other phases, that the SiO_2 abundance in the chromite-bearing points is still above 40 wt.% (Figure S14 in Supporting Information S1). We thus consider that low SiO_2 points (below 30 wt.%), with low Ca content (below 8 wt.%, inconsistent with Ca-sulfate) are likely carbonate bearing. They might simply not have been flagged as carbonate-bearing due to the conservative character of our criteria. In the Margin Unit, we thus have 31% of points which are potentially carbonate-bearing, following this reasoning. Finally, to also take into account the second limit mentioned above, and provide a less-constrained but more realistic estimate of the carbonate content in these rocks, we make the following hypotheses. First, we know that all points identified as carbonate-bearing must contain between 55 wt.% (L_c) and ∼95 wt.% carbonate, since we never identified pure carbonates. Second, we assume that the low-SiO_2, low-CaO points, which were determined above to likely contain carbonate despite not meeting the C/O criterion, likely have a carbonate abundance in the range 5–35 wt.% (equivalent of the missing SiO_2 in these points compared to olivine). With these hypotheses, we estimate the bulk carbonate content in the Margin Unit bedrock to be in the range 5–13 wt.% on average. We note that some points with more elevated SiO_2 content could also be carbonate-bearing, for example, if the LIBS footprint contains a mixture of carbonate and silica; however, we cannot assess such points. We thus consider that this is a reasonable, though rough, estimate, likely on the low side, of the carbonate content. Extending these estimates to the carbonate-bearing units and sub-units along the traverse, we get some quantitative evaluation of the carbonate abundance along the traverse: (a) lower limit of carbonate content based on percentage of identified carbonate-bearing points only; (b) percentage of possible carbonate-bearing points based on SiO_2 content; (c) estimated carbonate content assuming 55–95 wt.% and 5–35 wt.% carbonate in the identified and possible carbonate-bearing points, respectively (Table 3).

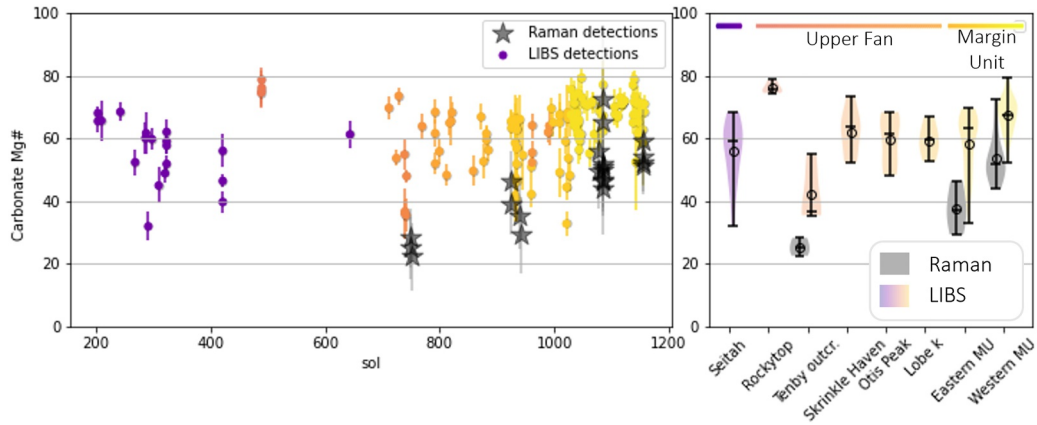

Figure 11. Multi-technique results: distribution and composition of carbonates along the traverse, as seen with LIBS and Raman. The colored markers and violins show LIBS results; Raman results are represented with gray stars and violins. For each violin, the median and mean values are represented with a dash and a circle, respectively. The Western-most MU is not represented as no carbonate was detected with LIBS, and the Raman detections there have a SNR below the threshold for Mg# derivation.

4.1.5. Carbonate Composition

The compositions of carbonates along the traverse derived from LIBS and Raman data are compared in Figure 11 (LIBS in color and Raman in gray). We note a good agreement between the techniques overall, with similar evolutions along the traverse (violin plot). The highest Mg# in the Upper Fan is found at Rockytop (no Mg# derived from Raman in this area). Then, except for the Tenby outcrop, which shows some interesting diversity of carbonates (detailed in Section 4.2.2), Mg# decreases progressively during the climb up the Fan. In the Margin Unit, it is the opposite: the Mg# is lower in the Eastern section, and is higher on average in the Western Margin. Note that this increase in Mg# between Eastern and Western Margin is consistent with a slight shift of the 2.5 µm band toward higher wavelengths observed in the VISIR data between these two sub-units, that is, not strong enough to be quantified.

The Raman-derived Mg# values are generally lower than those derived from LIBS. This is especially visible in the Eastern MU, where the Mg# observed in LIBS averages around 40 but the Raman measurements average around 60. Several parameters could explain this discrepancy. First, although Raman spectroscopy probes directly, and exclusively, the carbonate phase, the compositions reported with LIBS correspond to carbonates in mixtures, possibly including other FeO and/or MgO bearing mineral phases (SiO_2 typically above 10 wt.% in identified carbonate-bearing points, as shown in Figure 4). Moreover, previous analyses—based on comparison with the SuperCam calibration target as well as PIXL results—showed that the LIBS-derived Mg# of olivine is possibly slightly overestimated in Séítah (Beyssac et al., 2023), although it appears correct in Mg-rich olivine-rich boulders (Beyssac et al., 2026). Overall, we therefore give greater credit to the Raman-derived Mg# for carbonates, for absolute values, but refer to the LIBS for relative variations along the traverse, taking advantage of the larger number of observations. Moreover, with Raman, only the composition of carbonates could be quantified in this study, whereas LIBS provides composition information for all kind of targets along the traverse including bulk rocks as well as olivine. Using the MOC, we can thus compare the compositions of these different minerals and bulk rocks, benefiting from the relatively good precision (appropriate for relative comparisons) of the MOC (better than their accuracy, i.e., providing absolute values, R. Anderson et al., 2022).

In Figure 12, we compare the bulk composition with the compositions of carbonate and olivine detected in the different sub-units of the olivine-rich units explored by Perseverance, that is Séítah, the Upper Fan and the Margin Unit. Despite carbonate-bearing points detected with LIBS not being pure carbonates, their carbonate content (>55 wt% critical level L_c for detection, Table S6 in Supporting Information S1) ensures that the composition of the carbonate-bearing points is sufficiently affected by the composition of the carbonate themselves that their influence should be observable in these comparisons.

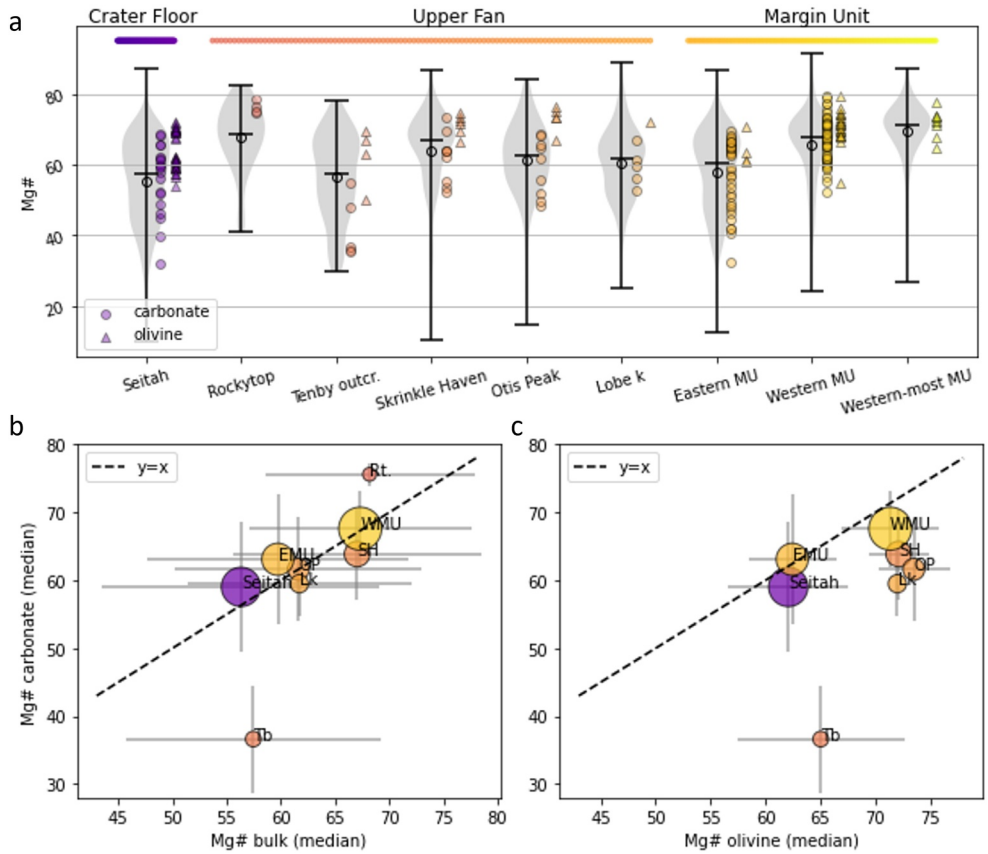

Figure 12. Comparing the LIBS-derived composition of bedrock, carbonate and olivine in the different olivine-bearing sub-units in Jezero Crater. (a) Composition of bedrock (gray violins, median shown with—and mean with o), carbonate (circles) and olivine (triangles) in the different olivine-bearing sub-units in Jezero Crater. No olivine was detected at Rockytop; no carbonate in the Western-most MU. (b, c) Scatter plots with median of the Mg# values in each sub-unit: (b) carbonate versus bulk rock; (c) carbonate versus olivine. The error bars represent the standard deviation of the distribution of Mg# values per sub-unit; the size of the markers is based on the number of bedrock observations in the sub-units. The color code and labels correspond to the sub-units: in the Upper Fan, Rt for Rockytop, Tb for the Tenby outcrop, SH for Skrinkle Haven, OP for Otis Peak, Lk for Lobe k; EMU and WMU for Eastern and Western Margin Unit, respectively. The dashed lines correspond to a 1:1 match.

Comparing the composition of the carbonates with the composition of the bulk rocks from LIBS data, we note that the composition of the carbonates are within the range of compositions (Mg# shown in Figure 12a) of other points in all sub-units along the traverse, and that the median composition of the bulk and carbonate match very well overall (Figure 12b). However, in some areas, the carbonates cover a significantly narrower range of Mg#. For example, at Rockytop (around sol 500), the Mg# of the carbonate is restricted to the highest part of the composition range observed in the bedrock. Conversely at Tenby (sols 733–752), carbonate compositions cover the lower end of Mg# values and the median composition of carbonate is significantly lower than the median bedrock composition.

Now comparing olivine and carbonate compositions (Figure 12a), there is a lack of Fe-rich olivine and Fe-rich carbonate in all considered units. We observe some carbonates with significantly lower Mg# than the olivine in most sub-units. However, the Western MU exhibits similar ranges of Mg# in both carbonate and olivine, both relatively Mg-rich, whereas the Eastern MU has Fe-rich carbonates compared to the olivine (see scatter of carbonate vs. olivine markers in upper plot). Overall the carbonates have Mg# similar or lower compared to the olivines (Figure 12c).

In the Margin Unit, we note that the observed increase of carbonate Mg# from East to West (Figure 11) is accompanied by an increase of bulk and olivine Mg# overall (Figure 12).

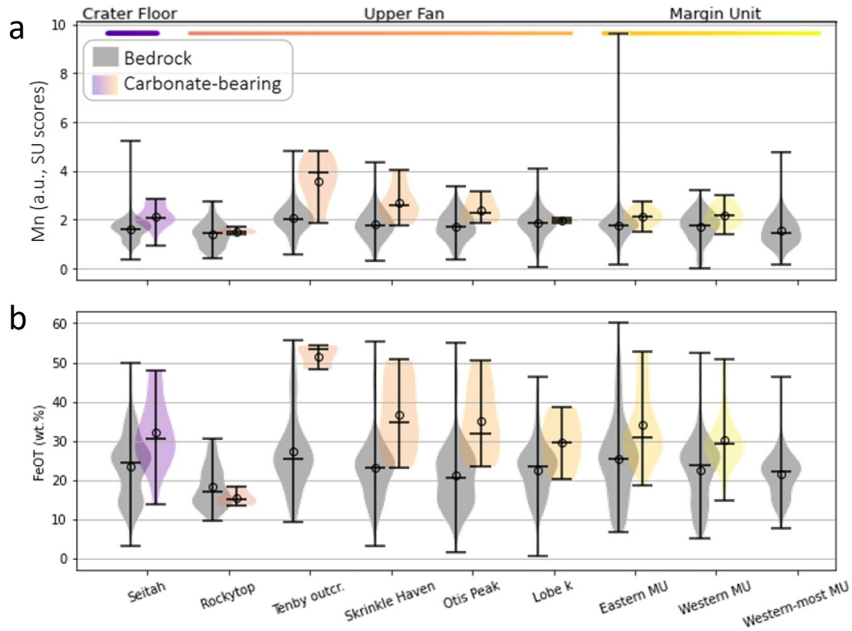

Figure 13. LIBS-derived carbonate compositions in Séítah, the Upper Fan and Margin with enhancements of Mn (based on SU scores, a) in Fe-rich carbonates (based on MOC, b) in the Tenby area (Tenby outcrop and a few points in the Skrinkle Haven member). Violin plots showing the distributions per sub-unit for all observations (gray) and carbonate-bearing points only (colored), with median (−) and mean (o) values.

4.2. Investigation of Specific Endmembers

4.2.1. Rockytop

The Rockytop outcrop (sols 476–499, Figure 1) is composed of conglomerates with subrounded granules and small pebbles dipping gently toward the south (Figure 2). Carbonates with high Mg# were detected with LIBS (Figure 12). A weak carbonate signature is also visible in the average Raman spectrum of the Thornton_Gap abraded patch, albeit with a low SNR (Figure 7 and spectrum in Figure S15 of Supporting Information S1). In the VISIR data, however, no 2.3 μm band is visible, despite the presence of a clear 2.5 μm band (Figure 8). A strong drop of absorption after 2.3 μm observed with this spectrum could indicate the presence of sulfate. It was shown that an intimate mixture of sulfate and carbonate can result in spectra with a 2.5 μm but no 2.3 μm spectra (Sheppard et al., 2024, 2025).

4.2.2. Fe-Mn-Rich Carbonates

At the beginning of the Upper Fan campaign, in the Skrinkle Haven member (and especially in the Tenby outcrop, Figure 1), some carbonate-bearing points present a relative enhancement in Mn, observable in LIBS with the Spectral Unmixing scores (Figure 13a). In that same area, carbonates were identified with very high FeO contents (around 50 wt.% FeO derived from LIBS, Figure 13b). This is consistent with the low Mg# observed in carbonates in that area (down to Mg# ∼35 with LIBS and around 25 with Raman, as seen in Figures 11 and 12). Note that presence of Mn in carbonates results in the main Raman mode shifting toward lower wavenumber, similar to Ca and Fe and away from the Mg endmember, resulting in an apparent lower Mg# (Bishop et al., 2021; Boulard et al., 2012). With more detailed analyses (presented in Supporting Information: Text S5 and Figures S17–S20 in Supporting Information S1, including images of these targets), the correlation between Fe and Mn is apparent at the point scale, and in the shot-to-shot data, confirming that the Mn is indeed associated with the Fe-rich carbonates in these points.

4.2.3. Magnesite Coatings/Fracture Fills

In the same area where Fe-Mn-rich carbonates were found, relatively lower wavelength positions of the 2.5 μm band unique signatures in VISIR spectra were indicative of particularly Mg-rich carbonate. For example,

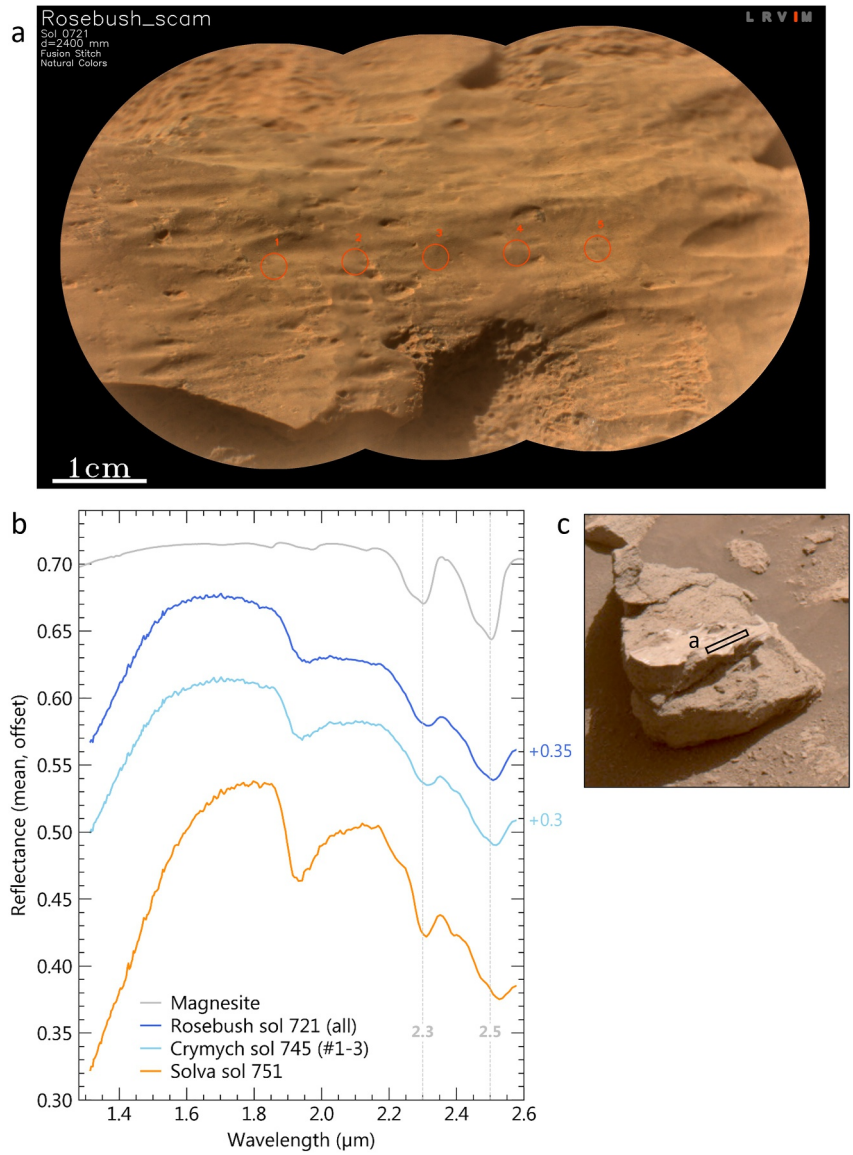

Figure 14. Observation of Mg-rich carbonate coatings or fracture fills in *Rosebush* and *Crymych*. (a) RMI mosaic of *Rosebush* with footprint of IRS analyses; (b) Average IRS spectra of Rosebush and *Crymych* targets, compared to a laboratory spectrum of magnesite and the average spectrum of *Solva* for reference. The dashed lines highlight variability in the positions of the 2.3 and 2.5 μm bands. (c) Context Mastcam-Z image for *Rosebush*. The black box corresponds to the location of the SuperCam target *Rosebush*, shown in panel (a).

Figure 14a shows that the 2.5 μm band in targets *Rosebush* and *Crymych* were shifted to lower wavelengths (similar to a laboratory spectrum of magnesite) compared to more Fe-rich carbonates such as *Solva*. The VISIR spectra of these two targets also show lower hydration than surrounding rocks, and the ratio of the 2.3 and 2.5 band depths is consistent with lower to no phyllosilicate contribution in these targets. For the two corresponding targets, these Mg-rich carbonates were detected on particular textures, likely corresponding to coatings or fracture fills (Figure 14; *Crymych* in Figure 2).

These two magnesite detections were found in outcrops where we also detected Fe-Mn-rich carbonates, at or close to the Tenby outcrop.

5. Discussion

5.1. Multi-Technique Analysis

We present a unique, multi-technique, in situ data set from a range of olivine, carbonate and silica bearing rocks. Despite the specific characteristics and limits of detections of each technique (discussed in details e.g., in Beck, Beyssac, et al., 2024; Clavé et al., 2023; Royer et al., 2025 as well as Table S6 in Supporting Information S1), they independently yield consistent results in terms of mineral distributions and chemical variations.

The multi-technique comparison in this study focused on outcrop, sub-unit and unit scale comparisons, since we already showed that point to point are both more challenging and less meaningful, considering the different sensitivities and different analytical footprints of the various techniques (Clavé et al., 2023). Compared to this previous study, the criteria for carbonate identification with LIBS are more conservative in the present work. This enables to make the results as robust as possible and limit the false detections to the minimum, while efficiently dealing with a large data set. This is enabled by the much higher carbonate abundances in the Upper Fan and Margin Unit compared to the Crater Floor. One consequence is a lower sensitivity to low carbonate abundances, which could hide some diversity of carbonates: in particular, we detect fewer carbonates in Máaz with these criteria compared to Clavé et al. (2023).

Despite none of our three techniques enabling quantitative characterization of carbonate mineral abundance at the point scale at this stage, we propose estimates based on the number of detections with LIBS and the sensitivity of this technique to carbonate.

5.2. Carbonate-Rich Rocks in Jezero Crater: Carbonation of Olivine-Rich Rocks

Using the three SuperCam techniques, we document the presence of carbonate along the traverse of the Perseverance rover in Jezero Crater. The carbonate in the crater floor igneous units, Máaz and Séítah were characterized in detail before (Clavé et al., 2023), we only include them for comparison. In the Fan Front, little to no carbonate was found in the bedrock (only some possible detections with VISIR but which are unclear and could not be confirmed by other techniques). The bulk rock composition in the Fan Front is more basaltic, with no olivine detected, suggesting a different source for the sediments and/or a contrasting style of alteration as sulfates and phyllosilicates dominate (Dehouck et al., 2024). This study is therefore focused on the Upper Fan and Margin Unit, which both present significant and ubiquitous olivine and carbonate.

The presence of carbonate has been assessed from orbital observations and was interpreted to be related to the local alteration in several areas of the regional olivine-rich unit (e.g., Ehlmann et al., 2008; Mandon et al., 2020). Our observations confirm these orbital detections of Mg-rich carbonate, as was already confirmed in situ in the crater floor (Clavé et al., 2023; Corpolongo et al., 2023; Farley et al., 2022; Liu et al., 2022; Scheller et al., 2022; Tice et al., 2022). In addition to orbital observations, we show: (a) that the Mg-rich carbonates are also iron-bearing and calcium-poor; (b) that the 2.2 micron band observed from orbit in the olivine- and carbonate-rich rocks (e.g., in Carter et al., 2023) is due to Si-OH rather than Al-OH in these units, as proposed for example by Tarnas et al. (2021) for certain areas; (c) that the relationship between olivine, carbonate and silica involves very fine-scale microtextural associations, since these phases are often observed as mixed in our analytic footprints (sub-millimetric to millimetric); (d) that carbonates could be even more widespread than observed from orbital data, especially in the Upper Fan, where they were only observed in certain areas/erosional windows from orbit (Ehlmann et al., 2008; Goudge et al., 2015) but are seen continuously in bedrock targets along the traverse with SuperCam. We also characterize the diversity of carbonates more precisely compared to orbital data thanks to the small analytical footprints of the instruments, frequent sampling along the rover traverse (analysis with SuperCam are performed at most rover stops) and the combination of different techniques with SuperCam providing better sensitivity. In particular, the carbonates observed in the sedimentary rocks of the delta and in the Margin Unit are more similar in composition than might have been expected from orbit. Moreover, the local identification of Fe-Mn-rich carbonates and magnesite could not be done from orbit.

In the Upper Fan and Margin Unit, carbonate is observed in the bulk of relatively coarse-grained rocks: they are pervasive and intimately mixed with olivine and silica. Although some Ca-sulfate and/or fluorite veins are locally observed in both units, carbonate is not detected in these veins. This rules out a mechanism of massive carbonate precipitation from fluids percolating in veins. Overall, the pervasive occurrence of carbonates and their co-occurrence with silica are consistent with olivine being transformed into an assemblage of carbonate and silica

according to the general reaction (Equation 1) (Kelemen, 2020; Kelemen et al., 2011). There is likely another Mg-rich silicate phase involved in the process like a Mg-rich clay (see below).

$$(Fe,Mg)_2SiO_4 + 2CO_2 \rightarrow 2(Fe,Mg)CO_3 + SiO_2 \quad (1)$$

Carbonate formation in the Upper Fan and Margin Unit, as in Séítah, thus appears consistent with in situ carbonation of ultramafic material. There are pyroxenes locally in the two units (high-Mg orthopyroxene to low-Ca pigeonite, Beyssac et al., 2026) but olivine is largely the dominant primary mineral in these rocks and olivine is more prone to alteration compared to low-calcium pyroxenes (Kelemen, 2020). We therefore assume that carbonate formation is mostly driven by carbonation of olivine. More specifically, the association of carbonate and silica in the three observed olivine-rich units indicates that a large part of the silica likely formed through the same process as most of the carbonate, and that neither of these phases was significantly dissolved and/or transported after partial dissolution of the olivine.

5.3. The Case of the Margin Unit

The nature of the Margin Unit and its relationship to the regional olivine-rich unit are still open for discussion. The olivine-rich protolith in the MU could originally be igneous (an olivine-rich cumulate?), pyroclastic (surge or flow?) or possibly sedimentary (originating from the regional olivine-rich unit or the rim of Jezero Crater) (Horgan, Garczynski, Barnes, et al., 2024; Williford et al., 2026).

Overall, the Margin Unit is distinctive due to its high compositional homogeneity, the uniquely low Al_2O_3, TiO_2, as well as low CaO, NaO_2 and KO_2 content in the bedrock. It is also characterized by three main groups of composition: (a) the ultramafic material composed by dominant olivine with pyroxene (mostly orthopyroxene to low-Ca pigeonite) and Cr-rich (Ti)-Fe oxides (possibly chromite and/or ulvöspinel, as also observed in Séítah and olivine-rich boulders on the Upper Fan characterized in Beyssac et al., 2023, 2026), (b) high Fe and Mg composition with low silica, a significant portion of which were confirmed as being dominated by carbonate, and (c) high silica points. VISIR observations also reveal the presence of some Fe-Mg clay minerals.

We distinguish three slightly different expressions of the Margin Unit as the rover crossed it from East to West: the Eastern, Western and Western-most areas, corresponding to increasing elevations along the inner part of the crater rim (Figure 1). The differences come from the structural position in the crater, the rock texture, bulk composition and inferred primary and secondary mineralogy.

Overall, our observations are consistent with the entire Margin Unit being a single unit with ultramafic primary composition and variable degree of alteration. The ultramafic protolith, could have been emplaced in situ as an igneous rock (as appears most likely in the West and Western-most parts in particular) or possibly be re-mobilized by sedimentary processes (proposed for the Eastern part, e.g., in Cardarelli et al., 2024; Horgan, Garczynski, Barnes, et al., 2024; Jones et al., 2024; Ravanis et al., 2024). Some subtle variability is also observed throughout the MU in the bulk rock composition, and especially in the composition of the olivine. The Mg# of bulk rocks in general, and of olivine minerals in particular, appears to increase with elevation along the Westwards rover traverse through the MU. This evolution could be related to a diversity of sources for the ultramafic protolith, or a single source becoming more evolved from West to East. A few strata or layers were observed in the Margin Unit with consistent shallow dipping to the east (Jones et al., 2024). Consequently, rocks to the West would correspond to stratigraphically lower layers. If the Margin Unit is sedimentary, Western rocks could be relatively older deposits, which could have been sourced from multiple areas with variable ultramafic composition. Alternatively, in an igneous scenario, the Western-most highest-elevation areas could actually correspond to deeper igneous rocks, which in the case of a single unit would then be expected to be less evolved at higher depth, which is consistent with our observations. Overall, we favor an igneous origin for the Western and Western-most MU with local remobilization in the Eastern MU.

The Eastern and Western MU constitute the most altered olivine-rich unit explored with Perseverance inside Jezero Crater. This is attested by the highest amounts of carbonate and high-silica points in LIBS data (Figure 10 and Table 3) as well as strong detections of carbonates in VISIR and Raman. Between these two areas, we note a difference in carbonate composition which shows some relation to the bulk rock composition. In the Western part, the composition of carbonates is within the (narrow) range of bulk rock composition in general, and olivine composition in particular. This, as the co-presence of olivine, carbonate and silica, is not consistent with the

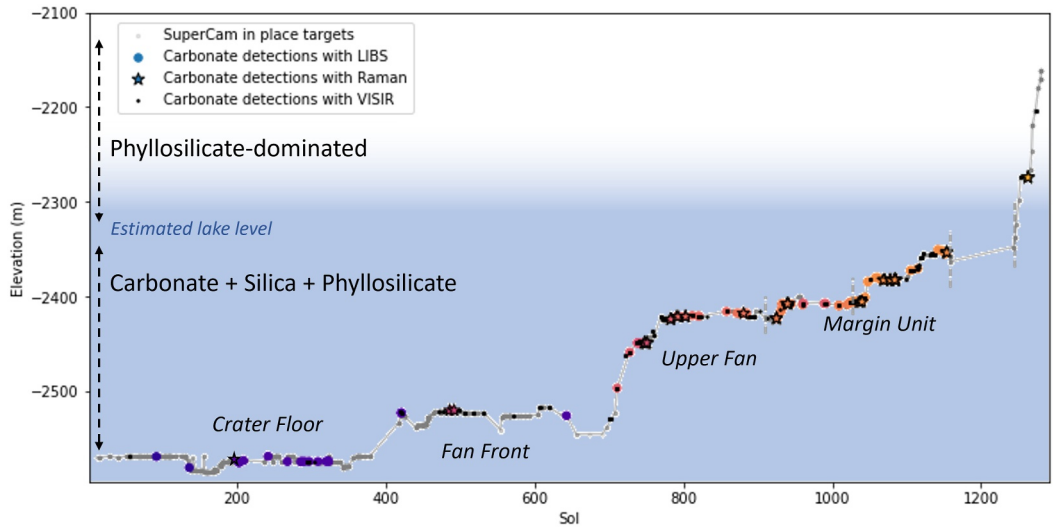

Figure 15. Overview of SuperCam carbonate detections along the traverse in Jezero Crater, as a function of target elevation. All bedrock targets analyzed with SuperCam are represented in gray. LIBS (colored circles), Raman (color stars with black edges) and VISIR (black dots) detections of carbonates in bedrock are represented. The estimated lake level corresponds to the values references in Figure 1.

expected sorting (chemical or mechanical) related to transport in sedimentary processes. No matter the emplacement process of these rocks, we thus consider that the carbonation in this area likely took place in situ, post emplacement of the rock. In the Eastern part, on the other hand, we observe carbonates with Mg# significantly lower than the olivine's in this area. This could indicate a significant external input locally. This input of Fe-rich carbonates could come either through Fe-rich fluids or detrital Fe-enriched carbonates. Considering that the Eastern MU plots follows the correlation between the abundances of carbonate and silica observed throughout in Jezero Crater (Figure 10), it is likely that this external input remains minor and that the majority of carbonates are not detrital. So the contribution of detrital Fe-enriched carbonate was probably not very significant overall, and we favor hypotheses involving a second phase of in situ alteration involving relatively Fe-rich fluids and/or preferential Mg-leaching.

Detection of carbonates in the Western-most MU is less evident: they are detected with Raman but not clearly with LIBS or VISIR in this area. The Raman data being too noisy, no carbonate composition could be derived for these few carbonates. On the other hand, Fe-Mg-phyllosilicates were observed all along the traverse with VISIR, but the carbonate-to-phyllosilicate ratio is clearly lower in the Western-most area. So the alteration style is different in the Western-most MU and could be related to difference in exposure to lake water. Indeed, the sedimentary rocks of the Upper Fan were deposited on top of the Eastern MU, and the Neretva Vallis channel incised both Eastern and Western MU, suggesting that these rocks were transiently in water and that fluid-rock interactions could occur. Consistently, the different lake levels derived from geomorphological observations span most of the Margin Unit elevations but the highest part of the Western-most MU was likely never under transient lake water and was just exposed to water runoff (Figures 1 and 15). On the other hand, similarly strong carbonate signatures are seen from orbit outside Jezero Crater, outside any crater (e.g., Mandon et al., 2020). The carbonates in these other locations of the regional olivine-rich unit, as well as the few carbonates observed at higher elevations in the Western-most MU, have therefore likely formed without the presence of a lake. It is therefore possible that similar processes may also have yielded heterogeneous yet locally intense carbonation of olivine-rich material within Jezero Crater, instead of or in complement to carbonation related to the presence of a lake.

Although SHERLOC detected locally some hydrated carbonate in the Eastern Margin unit (Srivastava et al., 2025), no evidence of such hydrated carbonate was found in the SuperCam data (details in Text S6; Figures S21 and S22 of Supporting Information S1). It is possible that SuperCam did not analyze the right spots, or that these hydrated carbonates are below the limits of detections of SuperCam techniques. In both cases, this suggests relatively minor amounts of hydrated carbonate compared to the anhydrous ones characterized in this study.

5.4. The Case of the Upper Fan

The Upper Fan consists of detrital sedimentary rocks, post-dating the Margin Unit, formed by fluvio-deltaic processes (e.g., Caravaca et al., 2024; Gupta et al., 2024; Gwizd et al., 2024; Mangold et al., 2021, 2023). These rocks show ubiquitous carbonate. The origin of these alteration minerals, as detrital components (allogenic) or formed in situ (authigenic) has been discussed in previous studies (e.g., Goudge et al., 2015). Considering the important similarities observed between the Upper Fan and the Margin Unit, in terms of bulk chemistry and mineralogy (e.g., Skrinkle Haven and the Western MU in Figure 12), as well as the granular texture (Figures 2 and 3), it is likely that the rocks of the Upper fan come from a source resembling the MU. Upper Fan rocks could consist either in (a) unaltered olivine-bearing sands altered post transport and deposition by aqueous processes, or (b) already altered carbonate-olivine bearing clasts. In the first case, the carbonation in the fan could be related to the overall aqueous activity during the fan emplacement and lake activity, and possibly somewhat coeval to that of the MU. In the second case, we should observe clasts of carbonates, something hard to distinguish based on SuperCam data alone. Still, the correlation observed in Figure 10 between the abundances of carbonate and silica, which holds in most of the Upper Fan indicates that, in the event of transport of carbonate and silica, sorting (chemical and mechanical both) must have been minimal, to not separate these two phases.

Two areas stand out and present different carbonate characteristics (composition) or mineral associations. First, the mineralogy of Rockytop, a granule conglomerate, appears distinct from the rest of the olivine-rich areas explored with Perseverance based on a weak olivine abundance, and a sulfate contribution in the bulk rock, unique among olivine-bearing rocks in Jezero Crater (Figures 8 and 10). From a geochemistry perspective, the carbonate-bearing points at Rockytop have some of the highest Mg# observed at Jezero Crater (Figure 12). Moreover, Rockytop is the only area where the Mg# of the carbonate is on average higher than that of the bulk rock, as observed with LIBS. Rockytop is interpreted as a deltaic foreset that was deposited unconformably on top of the sulfate-rich sandstones of Hogwallow Flats rocks (Stack et al., 2024), possibly before cementation of the Hogwallow Flats rocks. Hence, sulfates could have migrated by fluid circulation through the porosity of the sediments above, explaining the local presence of sulfates.

Second, the Tenby area, in the lower section of the Upper Fan shows some of the lowest Mg# observed in carbonates in the bedrock of the olivine-rich units (Figure 12). These carbonates have significantly lower Mg# than both bulk rock and olivine in the local bedrock. These Fe-rich carbonates also appear to be Mn-bearing (Section 4.2.2). On the other hand, magnesite fracture-fills have been observed in the same area (Section 4.2.3). These fills clearly indicate a process of dissolution-reprecipitation inside microfractures that occurred after the rock was already cemented. Their distinct Mg-composition and enhanced proportion of carbonates is thus likely related to a diagenetic process subsequent to the pervasive formation of Fe-rich carbonates within the rock. Additionally, the Tenby outcrop is the only olivine- and carbonate-rich area with no detection of silica with LIBS (Figure 10).

In summary, we conclude that the rocks of the Upper Fan derive from an olivine-rich source and contain carbonates and silica that are likely mostly authigenic products of an in situ carbonation process after transport and deposition. A detrital origin for these minerals transported from a MU-like source is an alternative possibility that might need returned samples to be discussed further, but, at this point, we disfavor it because of the high solubility of both carbonates and silica. Late-stage diagenetic processes including local dissolution of carbonates produced magnesite fracture fills and sulfate enrichment from the underlying sulfate-bearing Hogwallow Flat member at the base of the delta; for locations such as Rockytop.

5.5. Insights Into the Carbonation Process in the Margin Unit and Upper Fan

On Earth, carbonate is frequently found in association with olivine, due to olivine's low stability and tendency to alter when exposed to water and especially CO_2-rich fluids (e.g., Kelemen, 2020; Kelemen et al., 2011). Such associations are, in particular, observed in altered peridotite, with aqueous alteration generating mineral assemblages like magnesite—talc (e.g., Beinlich et al., 2010, 2020; Kelemen et al., 2022). Here, we hypothesize that most carbonates in the Margin Unit and Upper fan were formed from the in situ carbonation of olivine. We explore some physico-chemical aspects of the carbonation process based on the SuperCam data.

5.5.1. Preferential Carbonation of Olivine-Rich Rocks

In the Nili Fossae region, a general association of carbonate with olivine has been observed from orbit in previous studies (km-scale; e.g. Brown et al., 2020; Ehlmann et al., 2008; Mandon et al., 2020), now extended to smaller scales, providing some ground truth for orbital data. We mostly found carbonate in olivine-rich units (100–10 m-scale) and these phases also appear associated at the outcrop (m) and target (mm-cm) scales. Regarding this association, Gil-Lozano et al. (2024) highlighted the key role of bedrock composition in the formation of carbonates on Mars based on laboratory experiments. In particular, they showed that carbonates were only formed in their experiments upon alteration of olivine-bearing rocks; other protolith compositions could not neutralize the acidity of CO_2-rich atmosphere and thus reach a pH threshold necessary for carbonate precipitation. Similarly, no carbonate production was observed during experimental alteration of a basaltic Martian crust simulant which did not contain olivine (Baron et al., 2019). A similar explanation was proposed in Loche et al. (2024), where the described alteration experiments of olivine-rich basalt did not produce any carbonates either. To explain this, they proposed that, in addition to a pH threshold, a kinetic limit needs to be overcome: this can be achieved by an increase in weathering rate that produce an increase in alkalinity and of the activity of the carbonate forming cations, allowing sufficient supersaturation for the carbonates to precipitate (Tosca et al., 2018). In Jezero Crater, the high olivine abundance in the primary rocks compared to other terrains on Mars could result in a higher weathering rate, a faster increase in cation concentration, leading to higher activity of the carbonate forming cations and alkalinity.

5.5.2. Composition of Olivine and Carbonates

Many laboratory studies have studied the carbonation process of olivine in different conditions (e.g., Andreani et al., 2009; Cantando et al., 2008; Daval et al., 2013; Gil-Lozano et al., 2024; H. King et al., 2010; Kissick et al., 2021; Lacinska et al., 2016; Oelkers et al., 2018; Saldi et al., 2013; Wells et al., 2017). Carbonate precipitation was observed only for alteration of Mg-rich olivine (Gaudin et al., 2018; Gil-Lozano et al., 2024) but not for fayalite (Kissick et al., 2021). However, Gil-Lozano et al. (2024) showed that an enrichment in Fe in Martian olivines limits the quantity of carbonate but does not completely prevent its formation. Only Mg-carbonate was reported in these studies, no siderite, despite reported supersaturation of siderite in the fluids, leading to the hypothesis that the formation of siderite might be kinetically limited (Baron et al., 2019; Kissick et al., 2021; Loche et al., 2024). The relative composition of olivine and carbonate following the carbonation process thus appears to depend strongly on alteration conditions. This is also consistent with the models of Chevrier and Morisson (2021), which show that magnesite or siderite precipitate in different conditions, from lacustrine to hydrothermal.

In Jezero Crater, Mg-rich carbonates are found in association with Mg-rich olivine-bearing rocks, which is consistent with the laboratory studies. The fact that the carbonate found in Jezero Crater tend to be a little Mg-depleted compared to the olivine, but fits well the bulk composition of the rock, likely indicates the presence of a Mg-rich phase in the rocks, which raises the global Mg# compared to the olivine. No evidence of brucite was found with any of the SuperCam techniques (OH band in Raman, very high MgO abundances in LIBS or 2.33 μm absorption with VISIR, as described in Collet et al., 2025), although it might be hard to identify in mixtures. The MgO could be in the pyroxene (high-Mg orthopyroxene to high Mg low Ca pigeonite were found), or the phyllosilicates, which could bear the excess Mg coming from the olivine that was not included in carbonates. Since phyllosilicates are observed with little carbonate and silica in the Western-most MU than in the rest of the MU, this suggests that these different alteration phases were likely formed through two distinct alteration processes, or at least two distinct stages of an alteration event.

5.5.3. Porosity, Fluid Circulation and Volume Expansion During Carbonation

One key parameter to enable carbonation of ultramafic rocks is the diffusion/circulation of fluids enabling the alteration and carrying the carbon alkalinity. In many cases on Earth, altered ultramafic rocks present significant systems of fractures, in which fluid circulated and in which carbonates were deposited (e.g., Beinlich et al., 2020). In ophiolites, these fractures are generally related to extensive deformation and plate tectonic processes, which are not relevant to Mars. But the fracture system is also triggered and driven by the alteration process itself since incorporation of water or carbon induces significant volume expansion of the altered rock (+33% and +40% volume reported for serpentinization and carbonation of a rock, respectively; Kelemen et al., 2011; even higher

numbers are reported in Kelemen et al., 2022). Of course, the carbonation reaction in the Margin Unit and Upper Fan is far from complete but it has certainly affected the bulk volume of these rocks and their permeability.

On Earth, in addition to carbonate veins, carbonate can be found inside the matrix of the carbonated rocks, as observed for example, in the listvenite (fully carbonated ultramafic rock) in the Oman ophiolite (Beinlich et al., 2020). These are explained by the pervasive diffusion of CO_2-rich fluids through porosity through the rocks. This diffusion is however expectedly interrupted as the pores are filled with alteration products. The questions of connected porosity, compaction and fractures are thus key to understanding the carbonation process.

In the Upper Fan, the dominant lithology is sandstone with variable grain size. Sandstones generally have significant connected porosity, especially when the compaction is low, favorable to fluid circulation. Moreover, the identification of foreset and topset structures throughout the Upper Fan indicates that a large part of the rocks investigated with Perseverance in this area were deposited under water, as part of a delta prograding into a lake (Caravaca et al., 2024; Mangold et al., 2024a, 2024b). Abundant fluids could have thus altered these rocks to carbonate in situ after deposition. Caravaca et al. (2024) show that the deltaic structures observed on the Upper Fan likely correspond to the last stage of the lacustrine activity at Jezero Crater, with a decreasing lake level. Between burial of the detrital material by subsequent layers of sediments and this lake level decrease, we can explain the limited nature of the alteration, preserving some unaltered olivine grains and yielding a carbonate abundance estimated around 3–9 wt.%.

In the Margin Unit, the estimated 6–16 wt.% or 5–13 wt.% carbonate detected in the Eastern and Western MU, respectively are in the bulk of the rocks. No carbonate fracture fill or vein was observed at the resolution scale of our instruments. This likely indicates a pervasive diffusion of fluid through the connected pores and/or at the grain boundaries, rather than circulation through a fracture system. This requires some permeability of the original ultramafic protolith in the Margin Unit. If some of these rocks were deposited through sedimentary processes, as was proposed especially for the Eastern part, the same arguments as for the Upper Fan may apply here and alteration shortly after deposition and in poorly compacted rocks could explain this high carbonate content. If the Margin Unit were igneous initially, permeability could have been significant as well, depending on the exact nature of the rocks. In any case, we propose that any original porosity was filled by the volume expansion related to the carbonation process, explaining that the carbonation process stopped before full completion and that the rocks today appear massive, with no visible porosity at the resolution of our instruments. As mentioned before, this area of the Margin Unit was exposed to fluvial and/or lacustrine activity, attested by the overlying sedimentary rocks of the Upper Fan in the East, and the incision of the Neretva Vallis channel in the North. It is likely that the water related to this hydrologic activity played some role in the alteration of the Eastern and Western parts of the Margin Unit. However, in the Western and Eastern MU, the degree of alteration is higher compared to other places explored by Perseverance. Such extent of carbonation is challenging to solely explain through the interaction with a relatively dilute river or lake waters. The Western delta was estimated to have deposited within decades to century at most for the entire delta (Goudge et al., 2018; Ovchinnikova et al., 2025; Salese et al., 2020). This timescale is short compared to the alteration time of olivine grains, especially for weakly acidic to circumneutral pH at medium or low temperature (thousands to 10 of thousands of years to alter an olivine grain according to Stopar et al., 2006). This is consistent with the olivines grains being weathered in situ, potentially by a warmer and/or more acidic fluid. The fluids could have warmed by penetrating and diffusing at depth through the rocks, or maybe through local hydrothermalism processes to trigger fluid circulation and carbonation in the Eastern and Western Margin Unit. In the nearby crater rim unit which is older than the Margin Unit, Beck et al. (2025) recently evidenced an old, likely Noachian, hydrothermal system with circulation of hot waters responsible for the formation of various silica phases, from opal to quartz. Such hydrothermalism would likely not be related to the Jezero Crater impact itself because the olivine-rich unit drapes the eroded rim of Jezero Crater, implying some time between Jezero-forming impact and emplacement of this unit (Mandon et al., 2020). Moreover, if the Margin Unit had been emplaced before the Jezero impact, there would be evidence of deformation, displacement, fracturing, shock in the MU rocks which is not the case. However, there are many smaller craters in the area, and a later and smaller impact or a volcanic episode might have been enough to induce some hydrothermal activity. The proximity of the massive Isidis basin could also have played a role, leading to a thin crust and shallow hot mantellic material in the region sometimes possibly excavated by impacts (Beyssac et al., 2026; Neumann et al., 2004), which may be responsible for anomalously higher geothermal gradients in the area leading to the circulation of hot groundwaters. The precipitation of carbonate also requires a source of carbon, so it should be linked to the infiltration of carbon-rich water, originated from the atmosphere. Alternatively, it could be coming

from some magmatic activity in the region degassing CO_2, but it could also be mantellic CO_2 since the mantle is not far from the surface in the Isidis and Jezero region (Neumann et al., 2004). In any case, the association of clay and carbonate in most of the olivine-rich rocks from Séítah, the Upper Fan and the Margin Unit is consistent with low pCO2, based on the models of (Chevrier & Morisson, 2021).

5.5.4. Olivine Passivation Through Silica Precipitation

Noticeably, olivine is not completely transformed in the most altered rocks of the MU as observed in terrestrial listvenites. One hypothesis to explain the remaining olivine in the most carbonated rocks observed at Jezero could lie in the passivation process: a layer of silica forms around the olivine grain during alteration, preventing (or at least slowing down) subsequent dissolution of the olivine, and hence preserving some olivine. Previous studies showed the passivation of olivine requires some Fe in the olivine (Oelkers et al., 2018; Saldi et al., 2013), that magnesite then tends to form on the silica rather than an olivine surface (Johnson et al., 2014), and that an unconsolidated material was likely favorable to this passivation process, making it potentially less significant in rocks (Wells et al., 2017). Such silica could contribute to the high silica points in the LIBS data as well as to the Si-OH bands detected in VISIR spectra. In any case, olivine passivation is not the only process that could explain the remaining olivine: other parameters such as unfavorable kinetics, short duration of alteration, etc. could also play a role.

5.6. Implications for a Preliminary Carbon Budget in the Nili Fossae Regional Olivine-Rich Unit

This study provides a first estimate of the carbonate content for different olivine-rich units within Jezero Crater. Noticeably, carbonates were found in all these units although they have very contrasted orbital signatures with strong to low or even no carbonate contribution, that is, the Margin Unit compared to most of Séítah (Carter et al., 2023; Tarnas et al., 2021; Zastrow & Glotch, 2021). We propose to extrapolate these carbonate abundances to the regional olivine-rich unit, by making a few assumptions. We acknowledge the diversity of carbonate contribution observed from orbit in the regional olivine-rich unit in Nili Fossae (e.g., Mandon et al., 2020), and propose to derive lower and higher limits of carbonate content from the results presented in this work. For the higher limit, we consider the upper range of the approximate carbonate abundance estimated for the Eastern Margin Unit (Table 3), that is, 16 wt.% carbonate (see Section 4.1.4). Since this corresponds to some of the strongest carbonate signatures observed from orbit, we estimate that this value is a reasonable higher range for the overall regional unit. We assume that the lowest range of carbonate content estimated for the most carbonate-poor olivine regions presented in this study represent a lower average for the whole regional unit. We have indeed showed that regions with low to no carbonate signature from orbit might still have a small carbonate content detectable in situ. For the lower limit, we thus use the lower range of the approximate carbonate abundance estimated for Séítah and the Western-most Margin Unit (Table 3), that is, 1 wt.% carbonate.

Considering the surface of the regional olivine-rich unit of 18,000 km^2 (Mandon et al., 2020) and a thickness evaluated between 0.01 and 0.1 km (Kremer et al., 2019), we derive upper and lower values for the volume of this regional unit. We use an estimated density of 2,400–3,000 kg/m^3 based on the average Martian crust density (2,582 $\pm$ 209 kg/m^3, Wieczorek et al., 2022) and the expected density of an olivine cumulate like Séítah ($\sim$3,000 kg/m^3) to derive the equivalent mass. Using the lower and upper values for carbonate content in this unit, and assuming an average carbonate composition of Mg# 60 (consistent with Sections 4.1.4 and 4.1.5), we thus derive a carbon mass of 5.4×10^{11}–1.1×10^{14} kg C potentially stored in the regional olivine-rich unit as carbonate mineral. This represents 0.002%–0.4% of the current total mass of the atmosphere, stored in this region alone. Yet there are other olivine outcrops and carbonate detections elsewhere on Mars detected from orbit (e.g., Bishop et al., 2013; Carter et al., 2023; Michalski & Niles, 2010; Wray et al., 2016), suggesting that the quantity of carbon stored in rocks compared to the current mass of the atmosphere is likely significant. Overall, storage of atmospheric CO_2 in the form of carbonate minerals resulting from carbonation of ultramafic rocks on Mars may have played a global role for the Martian climate. This process may have contributed to the cooling of the Martian atmosphere by trapping and stabilizing atmospheric CO_2 within rocks over geological timescale.

5.7. Comparison to Other Martian Carbonates

5.7.1. Comanche Outcrop

The Algonquin class rocks in Columbia Hills, Gusev Crater were characterized as olivine-rich and interpreted as possible tephra deposits (McCoy et al., 2008; McSween et al., 2008). Fe-Mg carbonate and silica were also detected in nearby rocks, in the Comanche outcrop, and interpreted as likely related to hydrothermalism (Morris et al., 2010). A multi-step model was proposed, involving the dissolution of olivine in Algonquin class rocks and precipitation of carbonates in the Comanche outcrop (Ruff et al., 2014).

These rocks were compared to the olivine-rich unit in Nili Fossae, and it was proposed that they might share a similar origin: pyroclastic in Ruff et al. (2022), or as an olivine cumulate based on in situ observations of the Séítah formation in Jezero Crater (Beyssac et al., 2023 and references therein). The detection of silica and carbonates in both these places is another common factor. However, these alteration phases are spatially separated from the olivine in Gusev Crater, whereas the alteration and carbonate precipitation appear to have happened mostly in place in Jezero Crater.

5.7.2. Gale Crater

Carbonate and silica were detected in Gale crater. However, they were detected in distinct locations in the crater (Burtt et al., 2024; Frydenvang et al., 2017; Morris et al., 2016; Thorpe et al., 2022; Tutolo et al., 2024), not associated with olivine, and in much lower abundance than in Jezero Crater (Beck, Meslin, et al., 2024). Iron-rich carbonates were first detected as a minor phase (1%–3% ot total phases) by the CheMin X-ray diffractometer in sediments from the Glen Torridon area, in association with silicates and clay mineral (Thorpe et al., 2022). They were subsequently encountered higher in the stratigraphy, in a dark smooth layer referred to as the marker band. Carbonate minerals there were very close to the siderite endmember (Tutolo et al., 2024). Given the chemistry of the carbonate, and the geologic context, a formation by precipitation of lacustrine water, possibly related to evaporation of lake waters, has been proposed (Tutolo et al., 2024). Overall, carbonates encountered at Gale thus differ in their chemistry compared to those observed in Jezero Crater, and the associated paragenesis points toward different formation scenarios.

5.7.3. Martian Meteorites

Carbonates were identified in several Martian meteorites: carbonate-bearing hydrothermal veining in the clinopyroxene-rich nakhlites and different carbonates in Allan Hills (ALH) 84001, a piece of orthopyroxenite cumulate (Bridges et al., 2019). In ALH 84001, carbonates were shown to have formed at low temperatures (Halevy et al., 2011) and are associated with silica. These carbonates are thus consistent with the product of low-temperature alteration of an ultramafic rock like ALH 84001 or of clays formed by alteration of a mafic rock, in low water-to-rock ratio and mildly acidic conditions (Bridges et al., 2019).

In a previous study, we compared the composition of the carbonates identified with SuperCam in the floor of Jezero Crater with the compositions of the carbonates characterized in these Martian meteorites (Clavé et al., 2023). Similarly to the conclusions reported in this previous study, the Fe-Mg-rich, Ca-poor carbonates observed in Séítah, the Upper Fan and the Margin Unit are most similar to the Ca-poor fraction of carbonates characterized in ALH 84001. Moreover, the association of carbonate and silica in this meteorite is also comparable with our observations in Jezero Crater. Our interpretation of the Fe-Mg carbonates in Jezero Crater mostly originating from in situ carbonation of ultramafic rocks is consistent with the proposed origin of the carbonates in ALH 84001 (Clavé et al., 2023).

Between the Comanche outcrop and the ALH 84001 meteorite, we thus have two possible matches for the carbonates at Jezero. The proposed formation conditions for the carbonates in this outcrop and this meteorite are fairly different since hydrothermalism was proposed for Comanche, whereas low temperatures were derived for ALH 84001. This therefore does not help us much to constrain the conditions of the formation of the carbonates in Jezero Crater. We might not solve this question fully until we are able to analyze samples from Jezero in much greater detail in the laboratory.

5.8. Implications for Mars Sample Return

For the first time in Mars exploration, samples of the rocks analyzed in situ are being collected for a future return to Earth as part of the Mars Sample Return (MSR) program. To this end, two (pairs of) carbonate-bearing samples were collected in Séítah, three in the Upper Fan and three in the Margin Unit. Detailed analysis of these samples in the laboratory should help solve the remaining issues about these carbonates, among many other questions. Petrologic investigations down to the nanoscale should precise the inventory and the composition of all the mineral phases involved in this alteration process, primary and secondary mineral phases. A detailed micro-textural analysis should help precise the relation between the carbonates and olivines on one side, and carbonates and other alteration phases on the other side. Cathodoluminescence imaging should be used to precise the growth mechanism of these carbonates and identify possible different generations of carbonates due to successive fluid flows events. Isotopic (C, O) and trace elements geochemistry at the bulk rock scale as well as in situ at the grain scale should be instrumental to discuss the reservoirs involved, the fluxes as well to constrain the formation temperature of the carbonates. All these data on the various samples will help to constrain the nature of the protolith in terms of chemistry and mineralogy, and then the alteration process at work.

6. Conclusion

During the first three and a half years of the Mars 2020 mission, the Perseverance rover has explored in situ the three main olivine and carbonate-bearing units identified from orbit within Jezero Crater: (a) Séítah, an olivine cumulate in the crater floor, (b) the sedimentary rocks of the Upper Fan, and (c) a particularly carbonate-rich unit, identified as the "Marginal Carbonates" from orbit (Horgan et al., 2020) and called the Margin Unit in the scope of the Mars 2020 mission. The relationship between these units, their origin and the nature of the carbonates have been discussed extensively pre-Mars 2020 mission, based on orbital data (e.g., Brown et al., 2020; Edwards & Ehlmann, 2015; Ehlmann et al., 2008, 2009; Goudge et al., 2015; Horgan et al., 2020; Tarnas et al., 2021; Zastrow & Glotch, 2021).

We present the multi-technique data collected in situ on these olivine- and carbonate-bearing rocks with the SuperCam instrument: images, LIBS, Raman and VISIR data. These three units have mafic to ultramafic compositions, dominated by SiO_2, FeO and MgO and with overall low abundances in Al_2O_3, TiO_2, CaO, NaO_2 and K_2O. These rocks contain primary minerals with olivine, some pyroxene (orthopyroxene to low Ca pigeonite), and Cr-rich Ti-Fe oxides as well as secondary mineralogy related to alteration including Fe-Mg carbonates, clay minerals, and hydrated/hydroxylated silica. We used conservative criteria to identify olivine, carbonate-bearing and silica-rich points with LIBS, as well as carbonate with Raman and VISIR. We confirm the association of olivine and Fe-Mg carbonate observed from orbit and additionally show that carbonate are generally found in higher abundances in areas with fewer olivine. We also highlight a general correlation of the abundances of carbonate and silica in these three units. We interpret this as variable degrees of carbonation of olivine-rich rocks: Séítah being the least altered with 1–3 wt.% estimated carbonate content; then comes the Upper Fan with 3–9 wt.% estimated carbonate content and finally the Margin Unit with up to 6–16 wt.% carbonate content (in the Eastern MU). Only the Western-most, highest-elevation part of the Margin Unit shows evidence of different alteration: weaker and dominated by Fe-Mg phyllosilicate rather than carbonate. We compared the composition (Mg#) of the bulk, the olivine and the carbonate along the traverse. Despite uncertainties on absolute values derived from LIBS or Raman data, we observe some variability of composition along the traverse. In general, the composition of the carbonate matches very well with the bulk composition of local bedrock; the Mg# of carbonate is generally a little lower than that of the local olivine, though. Despite the different natures and emplacement mechanisms of the rocks in Séítah, the Upper Fan and the Margin Unit, we interpret the majority of the carbonates to have formed through the in situ alteration of ultramafic material. We also show evidence of later-stage dissolution and re-precipitation of carbonate in one specific area on the Upper Fan, highlighting multiple stages of carbonate mineralization in Jezero Crater.

The distribution of carbonate with elevation in the Upper Fan and Margin Unit suggests a contribution of the lacustrine activity to the carbonate process, possibly enhanced by hydrothermal activity. These in situ observations may be extrapolated to other carbonates-bearing rocks and would make the amount of carbon potentially stored in Martian ultramafic rocks overall significant. This would suggest that carbonation of ultramafic rocks might have played a key role in pumping CO_2 from and therefore in cooling the Martian atmosphere.

Conflict of Interest

The authors declare no conflicts of interest relevant to this study.

Availability Statement

The data in this publication are from the SuperCam instrument of the Mars 2020 Perseverance rover. The SuperCam data include the Laser Induced Breakdown Spectroscopy (LIBS), Visible/near infrared (VISIR) Spectroscopy, Time-Resolved Raman (TRR) spectroscopy and the Remote Micro-Imager (RMI). The SuperCam major element oxide composition (MOC), total emissivity, and all raw data and processed calibrated data files are included in the Planetary Data System (Wiens et al., 2021). In addition, all image data presented here from the, and SuperCam and Mastcam-Z instruments are available through the Planetary Data System Imaging Node (https://pds-imaging.jpl.nasa.gov/portal/mars2020_mission.html) and GeoSciences Node (https://pds-geosciences.wustl.edu/missions/mars2020/).

Acknowledgments
The authors gratefully acknowledge the Mars2020 and SuperCam Science and Engineering teams. E.C. thanks A. Lomashvili and C. Egerland for fruitful discussions. E.C., S.S., K.R., F.S. were supported by DLR. O.B., P.B., C.R., L.M., N.M., O.F., E.D., S.B., C.Q.N., M.L., G. C., T.F., S.M., P.-Y.M., S.LeM., P.P., C.P., O.G, A.C. were supported by CNES. O.F. was supported by INSU. C.Q.N. was supported by the European Research Council (ERC) under Horizon 2020 research and innovation programme (Grant 101045260). J.A., L.C., J.M.M. were supported by the Spanish AEI, grant PID2022-142750OB-I00. G.L.R., J.A.M. were supported by Spanish AEI and FEDER, European Union, Grants PID2022-142490OB-C32 and PCI2023-146000-2. Consejeria de Educación (JCyL) and FEDER Funds, Grants VA026G24 and CLU-2023-1-05. J.I.S was supported by Mars 2020 Science Office, NASA Mars Exploration Program. J.R.J. was supported by JPL subcontract 1532432. C.B., S.C. were supported by NASA grant NNH15AZ24I. R.C.W. was supported by NASA grant NNH13ZDA018O. Open access publication funding provided by COUPERIN CY26.

References

Allwood, A. C., Wade, L. A., Foote, M. C., Timothy, W. T., Hurowitz, J. A., Battel, S., et al. (2020). PIXL: Planetary instrument for X-ray lithochemistry. *Space Science Reviews*, *216*(8), 134. https://doi.org/10.1007/s11214-020-00767-7

Anderson, R. B., Forni, O., Cousin, A., Wiens, R. C., Clegg, S. M., Frydenvang, J., et al. (2022). Post-landing major element quantification using SuperCam laser induced breakdown spectroscopy. *Spectrochimica Acta Part B: Atomic Spectroscopy*, *188*, 106347. https://doi.org/10.1016/j.sab.2021.106347

Andreani, M., Luquot, L., Gouze, P., Godard, M., Hoisé, E., & Gibert, B. (2009). Experimental study of carbon sequestration reactions controlled by the percolation of CO_2-rich brine through peridotite. *Environmental Science & Technology*, *43*(4), 1226–1231. https://doi.org/10.1021/es8018429

Baron, F., Gaudin, A., Lorand, J.-P., & Mangold, N. (2019). New constraints on early Mars weathering conditions from an experimental approach on crust simulants. *Journal of Geophysical Research: Planets*, *124*(7), 1783–1801. https://doi.org/10.1029/2019JE005920

Beck, P., Beyssac, O., Dehouck, E., Bernard, S., Pineau, M., Mandon, L., et al. (2025). From hydrated silica to quartz: Potential hydrothermal precipitates found in Jezero Crater, Mars. *Earth and Planetary Science Letters*, *656*, 119256. https://doi.org/10.1016/j.epsl.2025.119256

Beck, P., Beyssac, O., Schmitt, B., Royer, C., Mandon, L., Boulard, E., et al. (2024). Quantification of crystal chemistry of Fe-Mg carbonates by Raman microspectroscopy and near-infrared remote sensing. *AGU Earth and Space Science*, *11*(9), e2024EA003666. https://doi.org/10.1029/2024EA003666

Beck, P., Forni, O., Lasue, J., Lewin, E., Cousin, A., Maurice, S., et al. (2016). Carbon detection with ChemCam: Laboratory studies and Mars results. In *47th Annual Lunar and Planetary Science Conference* (p. 1826).

Beck, P., Meslin, P., Fau, A., Forni, O., Gasnault, O., Lasue, J., et al. (2024). Detectability of carbon 1 with ChemCam LIBS: Distinguishing sample from Mars atmospheric carbon, and application to Gale crater. *Spectrochimica Acta Part B: Atomic Spectroscopy*, *408*, 115840. https://doi.org/10.1016/j.icarus.2023.115840

Beinlich, A., Austrheim, H., Glodny, J., Erambert, M., & Andersen, T. B. (2010). CO_2 sequestration and extreme Mg depletion in serpentinized peridotite clasts from the Devonian Solund basin, SW-Norway. *Geochimica et Coshmochimica Acta*. https://doi.org/10.1146/10.1016/j.gca.2010.07.027

Beinlich, A., Plümper, O., Boter, E., Müller, I. A., Kourim, F., Ziegler, M., et al. (2020). Ultramafic Rock Carbonation: Constraints from listvenite core BT1B, Oman Drilling Project. *Journal of Geophysical Research: Solid Earth*, *125*(6), e2019JB019060. https://doi.org/10.1029/2019JB019060

Bell, J. F., III., Maki, J. N., Mehall, G. L., Ravine, M. A., Caplinger, M. A., Bailey, Z. J., et al. (2021). The Mars 2020 perseverance rover mast camera zoom (Mastcam-Z) multispectral, stereoscopic imaging investigation. *Space Science Reviews*, *217*(1), 24. https://doi.org/10.1007/s11214-020-00755-x

Benzerara, K., Bernard, S., & Miot, J. (2018). Mineralogical identification of traces of life. In *Biosignatures for astrobiology. Advances in astrobiology and biogeophysics*. Springer.

Beyssac, O., Clavé, E., Forni, O., Udry, A., Pascuzzo, A., Dehouck, E., et al. (2026). Ultramafic float rocks at Jezero Crater (Mars): Excavation of lower crustal rocks or mantle peridotites by impact cratering? *Earth and Planetary Science Letters*, *675*, 119746. https://doi.org/10.1016/j.epsl.2025.119746

Beyssac, O., Forni, O., Cousin, A., Udry, A., Kah, L. C., Mandon, L., et al. (2023). Petrological traverse of an olivine-pyroxene cumulate on the floor of Jezero Crater, Mars: A perspective from SuperCam onboard perseverance. *Journal of Geophysical Research: Planets*, *128*(7), e2022JE007638. https://doi.org/10.1029/2022JE007638

Bhartia, R., Beegle, L. W., DeFlores, L., Abbey, W., Razzell Hollis, J., Uckert, K., et al. (2021). Perseverance's scanning habitable environments with Raman and luminescence for organics and chemicals (SHERLOC) investigation. *Space Science Reviews*, *217*(4), 58. https://doi.org/10.1007/s11214-021-00812-z

Bibring, J.-P., Langevin, Y., Gendrin, A., Gondet, B., Poulet, F., Berthé, M., et al. (2005). Mars surface diversity as revealed by the OMEGA/Mars Express observations. *Science*, *307*(5715), 1576–1581. https://doi.org/10.1126/science.1108806

Bishop, J. L., King, S. J., Lane, M. D., Brown, A. J., Lafuente, B., Hiroi, T., et al. (2021). Spectral properties of anhydrous carbonates and nitrates. *Earth and Space Science*, *8*(10), e2021EA001844. https://doi.org/10.1029/2021EA001844

Bishop, J. L., Tirsch, D., Tornabene, L. L., Jaumann, R., McEwen, A. S., McGuire, P. C., et al. (2013). Miineralogy and morphology of geologic units at Libya Montes, Mars: Ancient aqueously derived outcrops, mafic flows, fluvial features, and impacts. *Journal of Geophysical Research: Planets*, *118*(3), 487–513. https://doi.org/10.1029/2012JE004151

Bosak, T., Moore, K. R., Gong, J., & Grotzinger, J. P. (2021). Searching for biosignatures in sedimentary rocks from early Earth and Mars. *Nature Reviews Earth and Environment*, *2*(7), 490–506. https://doi.org/10.1038/s43017-021-00169-5

Boulard, E., Guyot, F., & Fiquet, G. (2012). The influence on Fe content on Raman spectra and unit cell parameters of magnesite–siderite solid solutions. *Physics and Chemistry of Minerals*, *39*(3), 239–246. https://doi.org/10.1007/s00269-011-0479-3

Boynton, W. V., Ming, D. W., Kounaves, S. P., Young, S. M. M., Arvidson, R. E., Hecht, M. H., et al. (2009). Evidence for calcium carbonate at the Mars Phoenix landing site. *Science*, *325*(5936), 61–64. https://doi.org/10.1126/science.1172768

Bramble, M. S., Mustard, J. F., & Salvatore, M. R. (2017). The geological history of Northeast Syrtis Major, Mars. *Icarus*, *293*, 66–93. https://doi.org/10.1016/j.icarus.2017.03.030

Bridges, J. C., Hicks, L. J., & Treiman, A. H. (2019). Carbonates on Mars. In *Volatiles in the Martian crust* (pp. 89–118). Elsevier. https://doi.org/10.1016/B978-0-12-804191-8.00005-2

Brown, A. J., Hook, S. J., Baldridge, A. M., Crowley, J. K., Bridges, N. T., Thomson, B. J., et al. (2010). Hydrothermal formation of Clay-Carbonate alteration assemblages in the Nili Fossae region of Mars. *Earth and Planetary Science Letters*, *297*(1–2), 174–182. https://doi.org/10.1016/j.epsl.2010.06.018

Brown, A. J., Viviano, C. E., & Goudge, T. A. (2020). Olivine-Carbonate mineralogy of the Jezero Crater Region. *Journal of Geophysical Research: Planets*, *125*(3), e2019JE006011. https://doi.org/10.1029/2019JE006011

Bultel, B., Viennet, J.-C., Poulet, F., Carter, J., & Werner, S. C. (2019). Detection of carbonates in Martian weathering profiles. *Journal of Geophysical Research*, *124*(4), 989–1007. https://doi.org/10.1029/2018JE005845

Burtt, D. G., Stern, J. C., Webster, C. R., Hofmann, A. E., Franz, H. B., Sutter, B., et al. (2024). Highly enriched carbon and oxygen isotopes in carbonate-derived CO_2 at Gale Crater, Mars. *Earth, Atmospheric and Planetary Sciences*, *121*(42), e2321342121. https://doi.org/10.1073/pnas.2321342121

Cantando, E. D., Dukes, C. A., Loeffler, M. J., & Baragiola, R. A. (2008). Aqueous depletion of Mg from olivine surfaces enhanced by ion irradiation. *Journal of Geophyscical Research*, *113*(E9). https://doi.org/10.1029/2008JE003119

Caravaca, G., Mangold, N., Williams, R. M. E., Barnes, R., Crumpler, L. S., Dromart, G., et al. (2024). Surface expressions and geometries of deltaic deposits of Jezero Western Fan top Mars. In *55th Lunar and Planetary Science Conference*.

Cardarelli, E. L., Artign, U., Paige, D. A., Russell, P., Hamran, S. E., Berger, T., et al. (2024). Ground penetrating rader illuminates sedimentary structures in the Mg-carbonate bearing Margin Unit of Jezero Crater. In *Tenth international conference on Mars 2024*.

Carter, J., Poulet, F., Bibring, J.-P., Mangold, N., & Murchie, S. (2013). Hydrous minerals on Mars as seen by the CRISM and OMEGA imaging spectrometers: Updated global view. *Journal of Geophysical Research: Planets*, *118*(4), 831–858. https://doi.org/10.1029/2012JE004145

Carter, J., Riu, L., Poulet, F., Bibring, P.-P., Langevin, Y., & Gondet, B. (2023). A Mars orbital catalog of aqueous alteration signatures (MOCAAS). *Icarus*, *389*, 115164. https://doi.org/10.1016/j.icarus.2022.115164

Chevrier, V. F., & Morisson, M. (2021). Carbonate-phyllosilicate parageneses and environments of aqueous alteration in Nili Fossae and Mars. *Journal of Geophysical Research: Planets*, *126*(4), e2020JE006698. https://doi.org/10.1029/2020JE006698

Clavé, E., Benzerara, K., Meslin, P., Forni, O., Royer, C., Mandon, L., et al. (2023). Carbonate detection with SuperCam in igneous rocks on the floor of Jezero Crater, Mars. *Journal of Geophysical Research: Planets*, *128*(6), e2022JE007463. https://doi.org/10.1029/2022JE007463

Collet, C., Cousin, A., Beyssac, O., Beck, P., Forni, O., Clegg, S., et al. (2025). Variably weathered ultramafic rocks: Investigation of their mineralogy with SuperCam-like techniques. *Spectrochimica Acta Part B: Atomic Spectroscopy*, *234*, 107338. https://doi.org/10.1016/j.sab.2025.107338

Corpolongo, A., Jakubek, R. S., Burton, A. S., Brown, A. J., Yanchilina, A., Czaja, A. D., et al. (2023). SHERLOC Raman mineral detections of the Mars 2020 Crater Floor campaign. *Journal of Geophysical Research: Planets*, *128*(3), e2022JE007455. https://doi.org/10.1029/2022JE007455

Cousin, A., Sautter, V., Fabre, C., Dromart, G., Montagnac, G., Drouet, C., et al. (2022). SuperCam calibration targets on board the perseverance rover: Fabrication and quantitative characterization. *Spectrochimica Acta Part B: Atomic Spectroscopy*, *188*, 106341. https://doi.org/10.1016/j.sab.2021.106341

Daval, D., Hellmann, R., Martinez, I., Gangloff, S., & Guyot, F. (2013). Lizardite serpentine dissolution as a function of pH and temperature, including effects of elevated pCO_2. *Chemical Geology*, *351*, 245–256. https://doi.org/10.1016/j.chemgeo.2013.05.020

Dehouck, E., Forni, O., Quantin-Nataf, C., Beck, P., Mangold, N., Beyssac, O., et al. (2024). Chemostratigraphy and mineralogy of the jezero Western fan as seen by the SuperCam instrument: Evidence for a complex aqueous history and variable alteration conditions. In *Tenth international conference on Mars 2024*.

Edwards, C. S., & Ehlmann, B. L. (2015). Carbon sequestration on Mars. *Geology*, *43*(10), 863–866. https://doi.org/10.1130/G36983.1

Ehlmann, B. L., Mustard, J. F., Murchie, S. L., Poulet, F., Bishop, J. L., Brown, A. J., et al. (2008). Orbital identification of carbonate-bearing rocks on Mars. *Science*, *322*(5909), 1828–1832. https://doi.org/10.1126/science.1164759

Ehlmann, B. L., Mustard, J. F., Swayze, G. A., Clark, R. N., Bishop, J. L., Poulet, F., et al. (2009). Identification of hydrated silicate minerals on Mars using MRO-CRISM: Geologic context near Nili Fossae and implications for aqueous alteration. *Journal of Geophysical Research*, *114*(E2). https://doi.org/10.1029/2009JE003339

Farley, K. A., Stack, K. M., Shuster, D. L., Horgan, B. H. N., Hurowitz, J. A., Tarnas, J. D., et al. (2022). Aqueously altered igneous rocks sampled on the floor of Jezero Crater, Mars. *Science*, *377*(6614), eabo2196. https://doi.org/10.1126/science.abo2196

Farmer, J. D., & Des Marais, D. J. (1999). Exploring for a record of ancient Martian life. *Journal of Geophysical Research*, *104*(E11), 26977–26995. https://doi.org/10.1029/1998JE000540

Fouchet, T., Reess, J. M., Montmessin, F., Hassen-Khodja, R., Nguyen-Tuong, N., Humeau, O., et al. (2022). The SuperCam infrared spectrometer for the perseverance rover of the Mars2020 mission. *Icarus*, *373*, 114773. https://doi.org/10.1016/j.icarus.2021.114773

Frydenvang, J., Gasda, P. J., Hurowitz, J. A., Grotzinger, J. P., Wiens, R. C., et al. (2017). Diagenetic silica enrichment and late-stage groundwater activity in Gale crater, Mars: Silica enriching diagenesis, Gale, Mars. *Geophysical Research Letters*, *44*(10), 4716–4724. https://doi.org/10.1002/2017GL073323

Gaillard, F., Michalski, J., Berger, J., McLennnan, S. M., & Scaillet, B. (2013). Geochemical reservoirs and timing of sulfur cycling on Mars. *Space Science Reviews*, *174*(1–4), 251–300. https://doi.org/10.1007/s11214-012-9947-4

Garczynski, B. J., Horgan, B. H. N., Johnson, J. R., Rice, M. S., Mandon, L., Chide, B., et al. (2025). Rock coatings as evidence for late surface alteration on the floor of Jezero Crater, Mars. *Journal of Geophysical Research: Planets*, *130*(9), e2025JE009242. https://doi.org/10.1029/2025JE009242

Garczynski, B. J., Ollila, A. M., Johnson, J., Farrand, W. H., Bedford, C. C., Gasda, P., et al. (2025). Summary of rock coating observations on Mars from past rover missions. In *56th Lunar and Planetary Science Conference*.

Gasnault, O., Mazoyer, J., Cousin, A., Meslin, P. Y., Lasue, J., Lacour, J. L., et al. (2012). Deciphering sample and atmosphere oxygen contents with ChemCam on Mars. In *43rd Annual Lunar and Planetary Science Conference* (p. 2888).

Gasnault, O., Virmontois, C., Maurice, S., Wiens, R. C., Le Mouélic, S., Bernardi, P., et al. (2021). What SuperCam will see: The remote micro-imager aboard perseverance. In *52nd Lunar and Planetary Science Conference*.

Gaudin, A., Dehouck, E., Grauby, O., & Mangold, N. (2018). Formation of clay minerals pn Mars: Insights from long-term experimental weathering of olivine. *Icarus*, *311*, 210–223. https://doi.org/10.1016/j.icarus.2018.01.029

Gil-Lozano, C., Baron, F., Gaudin, A., Lorand, J.-P., Fernandez, V., Hamon, J., & Mangold, N. (2024). The key role of bedrock composition in the formation of carbonates on Mars. *Geochemical Perspetives Letters*, *28*, 54–59. https://doi.org/10.7185/geochemlet.2403

Goudge, T. A., Head, J. W., Mustard, J. F., & Fassett, C. I. (2012). An analysis of open-basin lake deposits on Mars: Evidence for the nature of associated lacustrine deposits and post-lacustrine modification processes. *Icarus*, *219*(1), 211–229. https://doi.org/10.1016/j.icarus.2012.02.027

Goudge, T. A., Milliken, R. E., Head, J. W., Mustard, J. F., & Fassett, C. I. (2017). Sedimentological evidence for a deltaic origin of the western fan deposit in Jezero Crater, Mars and implications for future exploration. *Earth and Planetary Science Letters*, *458*, 357–365. https://doi.org/10.1016/j.epsl.2016.10.056

Goudge, T. A., Mohrig, D., Cardenas, B. T., & Fassett, C. I. (2018). Stratigraphy and paleohydrology of delta channel deposits, Jezero Crater, Mars. *Icarus*, *301*, 58–75. https://doi.org/10.1016/j.icarus.2017.09.034

Goudge, T. A., Mustard, J. F., Head, J. W., Fassett, C. I., & Wiseman, S. M. (2015). Assessing the mineralogy of the watershed and fan deposits of the Jezero Crater paleolake system, Mars: Jezero Paleolake System Mineralogy. *Journal of Geophysical Research: Planets*, *120*(4), 775–808. https://doi.org/10.1002/2014JE004782

Gupta, S., Stack-Morgan, K., Mangold, N., Ives, L. R. W., Gwizd, S., Caravaca, G., et al. (2024). Going with the flow: Sedimentary evolution of the Jezero Western Fan, Mars. In *55th Lunar and Planetary Science Conference*.

Gwizd, S., Stack, K. M., Ives, L., Gupta, S., Randazzo, N., Lamb, M., et al. (2024). Deposition history of the upper sequence of the Western Fan: Evidence for late-stage fluvial and potential igneous activity, Jezero Crater Mars. In *55th Lunar and Planetary Science Conference*.

Halevy, I., Fischer, W. W., & Eiler, J. M. (2011). Carbonates in the Martian meteorite Allan Hills 84001 formed at 18 pm 4°C in a near-surface aqueous environment. *Proceedings of the National Academy of Sciences*, *108*(41), 16895–16899. https://doi.org/10.1073/pnas.1109444108

Hamilton, V. E., & Christensen, P. R. (2005). Evidence for extensive, olivine-rich bedrock on Mars. *Geology*, *33*(6), 433. https://doi.org/10.1130/G21258.1

Hamran, S.-E., Paige, D. A., Andersson, P. F., Berger, T., Cardarelli, E., Carter, L., et al. (2024). RIMFAX ground penetrating radar observations of subsurface structures in Jezero Crater, Mars. In *Tenth international conference on Mars 2024*.

Hansen, P. (2022). *Modeling of LIBS sSpectra obtained in Martian Atmospheric Conditions* (PhD thesis). Humboldt-Universität zu Berlin.

Hermann, J., Gerhard, C., Burger, M., Craciun, V., & Pelascini, F. (2023). Progress in calibration-free laser-induced breakdown spectroscopy. *Spectrochimica Acta Part B: Atomic Spectroscopy*, *200*, 106595. https://doi.org/10.1016/j.sab.2022.106595

Hoefen, T. M., Clark, R. N., Bandfield, J. L., Smith, M. D., Pearl, J. C., & Christensen, P. R. (2003). Discovery of olivine in Nili Fossae Region of Mars. *Science*, *302*(5645), 627–630. https://doi.org/10.1126/science.1089647

Horgan, B. H. N., Anderson, R. B., Dromart, G., Amador, E. S., & Rice, M. S. (2020). The mineral diversity of Jezero Crater: Evidence for possible lacustrine carbonates on Mars. *Icarus*, *339*, 113526. https://doi.org/10.1016/j.icarus.2019.113526

Horgan, B. H. N., Garczynski, B., Barnes, R., Bedford, C., Cardarelli, E., Clavé, E., et al. (2024). Exploration of carbonate-rich rocks in the Margin Unit by the Perseverance rover in Jezero Crater. In *Tenth International Conference on Mars 2024*.

Horgan, B. H. N., Garczynski, B., Gupta, S., Jones, A., Barnes, R., Hurowitz, J., et al. (2024). Campaign overview and initial results from exploration of the Margin unit in Jezero Crater by the Perseverance rover. In *55th Lunar and Planetary Science Conference*.

Horgan, B. H. N., Udry, A., Rice, M., Alwmark, S., Amundsen, H. E. F., Bell, J. F., III., et al. (2023). Mineralogy, morphology, and emplacement history of the Maaz Formation on the Jezero Crater floor from orbital and rover observations. *Journal of Geophysical Research: Planets*, *128*(8), e2022JE007612. https://doi.org/10.1029/2022JE007612

Hurowitz, J. A., Tice, M. M., Allwood, A. C., Cable, M. L., Hand, K. P., Murphy, A. E., et al. (2025). Redox-driven mineral and organic associations in Jezero Crater, Mars. *Nature*, *645*(8080), 332–340. https://doi.org/10.1038/s41586-025-09413-0

Ives, E. R. W., Stack, K. M., Geyman, E. C., Gupta, S., Caravaca, G., Siebach, K. L., et al. (2025). Sedimentology and stratigraphy of the fluvial-deltaic Skrinkle Haven member, Tenby formation, Jezero Crater, Mars. *Journal of Sedimentary Research*, *95*(6), 1080–1113. https://doi.org/10.2110/jsr.2025.019

Jakosky, B. M., Brain, D., Chaffin, M., Curry, S., Deighan, J., Grebowsky, J., et al. (2018). Loss of the Martian atmosphere to space: Present-day loss rates determined from MAVEN observations and integrated loss through time. *Icarus*, *315*, 146–157. https://doi.org/10.1016/j.icarus.2018.05.030

Johnson, N. C., Thomas, B., Maher, K., Rosenbauer, R. J., Bird, D., & Brown, G. E. Jr. (2014). Olivine dissolution and carbonation under conditions relevant for in situ carbon storage. *Chemical Geology*, *373*, 93–105. https://doi.org/10.1016/j.chemgeo.2014.02.026

Jones, A. J., Gupta, S., Barnes, R., Horgan, B., Paar, G., Stack, K., et al. (2024). Stratigraphy and structure of the Margin Unit, Jezero Crater: Implications for formation settings. In *Tenth international conference on Mars 2024*.

Kelemen, P. B. (2020). Engineered carbon mineralization in ultramafic rocks for CO_2 removal from air: Review and new insights. *Chemical Geology*, *550*, 119628.

Kelemen, P. B., Carlos de Obeso, J., Leong, J. A., Godard, M., Okazaki, K., Kotowski, A. J., et al. (2022). Listvenite formation during mass transfer into the leading edge of mantel wedge: Initial results from Oman Drilling Project Hole BT1B. *Journal of Geophysical Research: Solid Earth*, *127*(2), e2021JB022352. https://doi.org/10.1029/2021JB022352

Kelemen, P. B., Matter, J., Streit, E. E., Rudge, J. F., Curry, W. B., & Blusztajn, J. (2011). Rates and mechanisms of mineral carbonation in peridotite: Natural processes and recipes for enhanced, in situ CO_2 capture and storage. In *Annual review of Earth and planetary sciences*. https://doi.org/10.1146/annurev-earth-092010-152509

King, H. E., Plümper, O., & Putnis, A. (2010). Effect of secondary phase formation on the carbonation of olivine. *Environmental Science & Technology*, *44*(16), 6503–6509. https://doi.org/10.1021/es9038193

Kissick, L. A., Mather, T. A., & Tosca, N. J. (2021). Unravelling surface and subsurface carbon sinks within the early Martian crust. *Earth and Planetary Science Letters*, *557*, 116663. https://doi.org/10.1016/j.epsl.2020.116663

Kite, E. S., Gao, P., Goldblatt, C., Mischna, M. A., Mayer, D. P., & Yung, Y. L. (2017). Methane bursts as a trigger for intermittent lake-forming climates on Post-Noachian Mars. *Nature Geoscience*, *10*(10), 737–740. https://doi.org/10.1038/ngeo3033

Kite, E. S., Steele, L. J., Mischna, M. A., & Richardson, M. I. (2021). Warm early Mars surface enabled by high-altitude water ice clouds. *Proceedings of the National Academy of Sciences*, *118.18*(18), e2101959118. https://doi.org/10.1073/pnas.2101959118

Kremer, C. H., Mustard, J. F., & Bramble, M. S. (2019). A widespread olivine-rich ash deposit on Mars. *Geology*, *47*(7), 677–681. https://doi.org/10.1130/G45563.1

Kronyak, R. E., Stack, K. M., Sholes, S. F., Sun, V. Z., Gupta, S., Shuster, D. L., & Caravaca, G. (2023). Geomorphology and relative ages of channel belt deposits in Jezero's Western delta. In *54th Lunar and Planetary Science Conference*.

Kuebler, K. E., Jolliff, B. L., Wang, A., & Haskin, L. A. (2006). Extracting olivine (Fo-Fa) compositions from Raman spectral peak positions. *Geochimica et Cosmochimica Acta*, *70*(24), 6201–6222. https://doi.org/10.1016/j.gca.2006.07.035

Lacinska, A. M., Styles, M. T., Bateman, K., Wagner, D., Hall, R. H., Gowing, C., & Brown, P. D. (2016). Acid-dissolution of antigorite, chrysotile and lizardite for ex situ carbon capture and storage by mineralization. *Chemical Geology*, *437*, 153–169. https://doi.org/10.1016/j.chemgeo.2016.05.015

Lammer, H., Chassefière, E., Karatekin, O., Morschhauser, A., Niles, P. B., Mousis, O., et al. (2013). Outgassing history and escape of the Martian atmosphere and water inventory. *Space Science Reviews*, *174*(1), 113–154. https://doi.org/10.48550/arXiv.1506.06569

Lapo, K. E., Vaughan, A., Rice, M. S., Mandon, L., Johnson, J. R., & Garczynski, B. J. (2024). Distinguishing iron carbonates from olivines in visible to near-infrared Mastcam-Z spectra. In *55th Lunar and Planetary Science Conference*.

Lasue, J., Cousin, A., Meslin, P., Mangold, N., Wiens, R. C., Berger, G., et al. (2018). Martian eolian dust probed by ChemCam. *Geophysical Research Letters*, *45*, 20. https://doi.org/10.1029/2018GL079210

Leshin, L. A., Mahaffy, P. R., Webster, C. R., Cabane, M., Coll, P., Conrad, P. G., et al. (2013). Volatile, isotope, and organic analysis of Martian fines with the Mars curiosity rover. *Science*, *341*(6153), 1238937. https://doi.org/10.1126/science.1238937

Liu, Y., Tice, M. M., Schmidt, M. E., Treiman, A. H., Kizovski, T. V., Hurowitz, J. A., et al. (2022). An olivine cumulate outcrop on the floor of Jezero Crater, Mars. *Science*, *377*(6614), 1513–1519. https://doi.org/10.1126/science.abo2756

Loche, M., Fabre, S., Cousin, A., Proietti, A., Rapin, W., Tutolo, B. M., et al. (2024). Enhanced mobility of iron and manganese on mars: Evidence from kinetic experiments and models. *Chemical Geology*, *662*, 122242. https://doi.org/10.1016/j.chemgeo.2024.122242

Lopez-Reyes, G., Manrique, J. A., Clavé, E., Ollila, A., Beyssac, O., Pilleri, P., et al. (2025). Supercam Raman activities at Jezero Crater, Mars: Observational strategies, data processing, and mineral detections during the first 1000 sols. *Journal of Geophysical Research: Planets*, *130*(11), e2025JE008943. https://doi.org/10.1029/2025JE008943

Mandon, L., Ehlmann, B. L., Wiens, R. C., Garczynski, B. J., Horgan, B. H. N., Fouchet, T., et al. (2024). Variable iron mineralogy and redox conditions recorded in ancient rocks measured by in situ Visible/near-infrared spectroscopy at Jezero Crater, Mars. *Journal of Geophysical Research: Planets*, *129*(7), e2023JE008254. https://doi.org/10.1029/2023JE008254

Mandon, L., Quantin-Nataf, C., Royer, C., Beck, P., Fouchet, T., Johnson, J. R., et al. (2023). Reflectance of Jezero Crater floor: 2. *Journal of Geophysical Research: Planets*, *128*(7), e2022JE007450. https://doi.org/10.1029/2022JE007450

Mandon, L., Quantin-Nataf, C., Thollot, P., Mangold, N., Lozac'h, L., Dromart, G., et al. (2020). Refining the age, emplacement and alteration scenarios of the olivine-rich unit in the Nili Fossae region, Mars. *Icarus*, *336*, 113436. https://doi.org/10.1016/j.icarus.2019.113436

Mangold, N., Caravaca, G., Gupta, S., Williams, R. M. E., Dromart, G., Gasnault, O., et al. (2023). The formation of the fluvio-deltaic deposits of the western fan of Jezero Crater, Mars, during lake-level fall. In *AGU fall meeting*.

Mangold, N., Caravaca, G., Gupta, S., Williams, R. M. E., Gasnault, O., Le Mouélic, S., et al. (2024a). Constraints on Jezero paleolake history from its fluvial input. In *Tenth international conference on Mars 2024*.

Mangold, N., Caravaca, G., Gupta, S., Williams, R. M. E., Gasnault, O., Le Mouélic, S., et al. (2024b). Past variations of water level of Jezero paleolake. In *55th Lunar and Planetary Science Conference*.

Mangold, N., Gupta, S., Gasnault, O., Dromart, G., Tarnas, J. D., Sholes, S. F., et al. (2021). Perseverance rover reveals an ancient Delta-Lake system and flood deposits at Jezero Crater, Mars. *Science*, *374*(6568), 711–717. https://doi.org/10.1126/science.abl4051

Manning, C., Mckay, C., & Zahnle, K. (2006). Thick and thin models of the evolution of carbon dioxide on Mars. *Icarus*, *180*(1), 38–59. https://doi.org/10.1016/j.icarus.2005.08.014

Maurice, S., Clegg, S. M., Wiens, R. C., Gasnault, O., Rapin, W., Forni, O., et al. (2016). ChemCam activities and discoveries during the nominal mission of the Mars Science Laboratory in Gale crater, Mars. *Journal of Analytical Atomic Spectrometry*, *31*(4), 863–889. https://doi.org/10.1039/C5JA00417A

Maurice, S., Wiens, R. C., Bernardi, P., Caïs, P., Robinson, S., Nelson, T., et al. (2021). The SuperCam instrument suite on the Mars 2020 rover: Science objectives and mast-unit description. *Space Science Reviews*, *217*(3), 47. https://doi.org/10.1007/s11214-021-00807-w

McCoy, T. J., Sims, M., Schmidt, M. E., Edwards, L., Tornabene, L. L., Crumpler, L. S., et al. (2008). Structure, stratigraphy, and origin of Husband Hill, Columbia Hills, Gusev Crater, Mars. *Journal of Geophysical Research*, *113*(E6). https://doi.org/10.1029/2007JE003041

McSween, H. Y., Ruff, S. W., Morris, R. V., Gellert, R., Klingelhöfer, G., Christensen, P. R., et al. (2008). Mineralogy of volcanic rocks in gusev crater, Mars: Reconciling mössbauer, alpha particle X-Ray spectrometer, and miniature thermal emission spectrometer spectra. *Journal of Geophysical Research*, *113*(E6). https://doi.org/10.1029/2007JE002970

Meslin, P.-Y., Forni, O., Beck, P., Cousin, A., Beysac, O., Lopez-Reyes, G., et al. (2022). Evidence for perchlorate and sulfate in Jezero Crater, Mars, from SuperCam observations. In *53rd Lunar and Planetary Science Conference*.

Meslin, P.-Y., Gasnault, O., Forni, O., Schröder, S., Cousin, A., Berger, G., et al. (2013). Soil diversity and hydration as observed by ChemCam at Gale Crater, Mars. *Science*, *341*(6153), 1238670. https://doi.org/10.1126/science.1238670

Michalski, J. R., & Niles, P. B. (2010). Deep crustal carbonate rocks exposed by meteor impact on Mars. *Nature Geoscience*, *3*(11), 751–755. https://doi.org/10.1038/ngeo971

Morris, R. V., Ruff, S. W., Gellert, R., Ming, D. W., Arvidson, R. E., Clark, B. C., et al. (2010). Identification of carbonate-rich outcrops on Mars by the Spirit Rover. *Science*, *329*(5990), 421–424. https://doi.org/10.1126/science.1189667

Morris, R. V., Vaniman, D. T., Blake, D. F., Gellert, R., Chipera, S. J., Rampe, E. B., et al. (2016). Silicic volcanism on Mars evidenced by tridymite in high-SiO_2 sedimentary rock at Gale crater. *Proceedings of the National Academy of Sciences*, *113*(26), 7071–7076. https://doi.org/10.1073/pnas.1607098113

Mustard, J. F., Poulet, F., Head, J. W., Mangold, N., Bibring, J.-P., Pelkey, S. M., et al. (2007). Mineralogy of the Nili Fossae region with OMEGA/Mars Express data: 1. Ancient impact melt in the Isidis Basin and implications for the transition from the Noachian to Hesperian. *Journal of Geophysical Research*, *112*, E8. https://doi.org/10.1029/2006JE002834

Nachon, M., Lopez-Reyes, G., Meslin, P.-Y., Ollila, A., Mandon, L., Clavé, E., et al. (2023). Light-toned veins and material in Jezero Crater, Mars, as seen in-situ via NASA's Perseverance Rover (Mars 2020 mission): Stratigraphic distribution and compositional results. In *54th Lunar and Planetary Science Conference*.

Nachon, M., Siebach, K. L., Sholes, S., Sun, V. Z., Del Sesto, T., Weiss, B. P., et al. (2024). Overview of the Mars 2020 mission Perseverance rover third science campaign: Exploring Jezero Crater's upper Fan. In *55th Lunar and Planetary Science Conference*.

Neumann, G. A., zuber, M. T., Wieczorek, M. A., McGovern, P. J., Lemoine, F. G., & Smith, D. E. (2004). Crustal structure of Mars from gravity and topography. *Journal of Geophysical Research*, *109*(E8). https://doi.org/10.1029/2004JE002262

Newville, M., Otten, R., Nelson, A., Stensitzki, T., Ingargiola, A., Allan, D., et al. (2025). LMFIT: Non-linear least-squares minimization and curve-fitting for python. https://doi.org/10.5281/zenodo.15014437

Niles, P. B., Catling, D. C., Berger, G., Chassefière, E., Ehlmann, B. L., Michalski, J. R., et al. (2013). Geochemistry of carbonates on Mars: Implications for climate history and nature of aqueous environments. *Space Science Reviews*, *174*(1–4), 301–328. https://doi.org/10.1007/s11214-012-9940-y

Oelkers, A. H., Declercq, J., D Saldi, G., Gislason, S. R., & Schott, J. (2018). Olivine dissolution rates: A critical review. *Chemical Geology*, *500*, 1–19. https://doi.org/10.1016/j.chemgeo.2018.10.008

Ovchinnikova, A., Jaumann, R., G Walter, S. H., Gross, C., Zuschneid, W., & Postberg, F. (2025). A modeling approach for water and sediment transport in Jezero Crater on Mars based on new geomorphological evidence. *Icarus*, *426*, 116349. https://doi.org/10.1016/j.icarus.2024.116349

Palumbo, A. M., & Head, J. W. (2017). Impact cratering as a cause of climate change, surface alteration, and resurfacing during the early history of Mars. *Meteoritics & Planetary Sciences*, *53*(4), 687–725. https://doi.org/10.1111/maps.13001

Poggialini, F., Campanella, B., Cocciaro, B., Lorenzetti, G., Palleschi, V., & Legnaioli, S. (2023). Catching up on calibration-free LIBS. *Journal of Analytical Atomic Spectrometry*, *38*(9), 1751–1771. https://doi.org/10.1039/D3JA00130J

Ramirez, R. M., & Craddock, R. A. (2018). The geological and climatological case for a warmer and wetter early Mars. *Nature Geoscience*, *11*(4), 230–237. https://doi.org/10.1038/s41561-018-0093-9

Rapin, W., Meslin, P. Y., Maurice, S., Wiens, R., Laporte, D., Chauviré, B., et al. (2017). Quantification of water content by laser-induced breakdown spectroscopy on Mars. *Spectrochimica Acta Part B: Atomic Spectroscopy*, *130*, 82–100. https://doi.org/10.1016/j.sab.2017.02.007

Ravanis, E., Bedford, C., Garczynski, B., Horgan, B., Jones, A., Johnson, J., et al. (2024). Investigating rock textures and diagenetic features across the Margin UNit, Jezero Crater using mastcam-Z and SuperCam data. In *Tenth international conference on Mars 2024*.

Rogers, A. D., Warner, N. H., Golombek, M. P., Head, J. W. I. I. I., & Cowart, J. C. (2018). Areally extensive surface bedrock exposures on Mars: Many are clastic rocks, not Lavas. *Geophysical Research Letters*, *45*(4), 1767–1777. https://doi.org/10.1002/2018GL077030

Royer, C., Fouchet, T., Mandon, L., Montmessin, F., Poulet, F., Forni, O., et al. (2023). Reflectance of Jezero Crater floor: 1. Data processing and calibration of the Infrared Spectrometer (IRS) on SuperCam. *Journal of Geophysical Research: Planets*, *128*, e2022JE007481. https://doi.org/10.1029/2022JE007481

Royer, C., Poulet, F., Wiens, R., Montmessin, F., Beck, P., Beyssac, O., et al. (2025). The mineralogical composition of Jezero Crater Western Fan: Multigaussian modeling of Perseverance/SuperCam near-infrared observations and overview of major units. *Icarus*, *434*, 116538. https://doi.org/10.1016/j.icarus.2025.116538

Ruff, S. W., Hamilton, V. E., Rogers, A. D., Edwards, C. S., & Horgan, B. H. (2022). Olivine and carbonate-rich bedrock in Gusev crater and the Nili Fossae region of Mars may be altered ignimbrite deposits. *Icarus*, *380*, 114974. https://doi.org/10.1016/j.icarus.2022.114974

Ruff, S. W., Niles, P. B., Alfano, F., & Clarke, A. B. (2014). Evidence for a Noachian-aged ephemeral lake in Gusev crater, Mars. *Geology*, *42*(4), 359–362. https://doi.org/10.1130/G35508.1

Saldi, G. D., Daval, D., Morvan, G., & Knauss, K. G. (2013). The role of Fe and redox conditions in olivine carbonation rates: An experimental study of the rate limiting reactions at 90 and 150°C in open and closed systems. *Geochimica et Cosmochimica Acta*, *118*, 157–183. https://doi.org/10.1016/j.gca.2013.04.029

Salese, F., Kleinhans, M. G., Mangold, N., Ansan, V., McMahon, W., de Haas, T., & Domart, G. (2020). Estimated minimum life span of the Jezero fluvial Delta (Mars). *Astrobiology*, *20*(8), 977–993. https://doi.org/10.1089/ast.2020.2228

Scheller, E. L., Swindle, C., Grotzinger, J., Barnhart, H., Bhattacharjee, S., Ehlmann, B. L., et al. (2021). Formation of magnesium carbonates on Earth and implications for Mars. *Journal of Geophysical Research*, *126*(7), e2021JE006828. https://doi.org/10.1029/2021JE006828

Scheller, E. L., Razzell Hollis, J., Cardarelli, E. L., Steele, A., Beegle, L. W., Bhartia, R., et al. (2022). Aqueous alteration processes in Jezero Crater, Mars – Implications for organic geochemistry. *Science*, *378*(6624), 1105–1110. https://doi.org/10.1126/science.abo5204

Schon, S. C., Head, J. W., & Fassett, C. I. (2012). An overfilled lacustrine system and progradational delta in Jezero Crater, Mars: Implications for Noachian climate. *Planetary and Space Science*, *67*(1), 28–45. https://doi.org/10.1016/j.pss.2012.02.003

Schröder, S., Clavé, E., Hansen, P. B., Rammelkamp, K., Seel, F., Hubers, H.-W., et al. (2024). Minor and trace element enhancements identified in SuperCam LIBS data with spectral unmixing. In *55th Llunar and Planetary Science Conference*.

Schröder, S., Meslin, P. Y., Gasnault, O., Maurice, S., Cousin, A., Wiens, R., et al. (2015). Hydrogen detection with ChemCam at Gale Crater. *Icarus*, *249*, 43–61. https://doi.org/10.1016/j.icarus.2014.08.029

Schröder, S., Rammelkamp, K., Vogt, D. S., Gasnault, O., & Hübers, H.-W. (2019). Contribution of a martian atmosphere to laser-induced breakdown spectroscopy (LIBS) data and testing its emission characteristics for normalization applications. *Icarus*, *325*, 1–15. https://doi.org/10.1016/j.icarus.2019.02.017

Sharma, S. K., Misra, A. K., Lucey, P. G., Wiens, R. C., & Clegg, S. M. (2007). Combined remote LIBS and Raman spectroscopy at 8.6m of sulfur-containing minerals, and minerals coated with hematite or covered with basaltic dust. *Spectrochimica Acta Part A: Molecular and Biomolecular Spectroscopy*, *68*(4), 1036–1045. https://doi.org/10.1016/j.saa.2007.06.046

Sheppard, R. Y., Loizeau, D., Fraeman, A. A., Rampe, E. B., Pilorget, C., & Bibring, J.-P. (2025). The presence of Mg-sulfate can obscure spectral evidence of siderite. In *56th Lunar and Planetary Science Conference*.

Sheppard, R. Y., Loizeau, D., Rampe, E. B., & Fraeman, A. A. (2024). The presence of Mg-sulfate can obscure the spectral evidence of siderite. In *55th Lunar and Planetary Science Conference*.

Shields, G. A. (2007). Chapter 7.6—The marine Carbonate and Chert isotope records and their implications for tectonics, life and climate on the early Earth. *Developments in Precambrian Geology*, 971–983. https://doi.org/10.1016/S0166-2635(07)15076-3

Srivastava, A., Steel, A., Kah, L. C., Conrad, P. G., Sharma, S., Phua, Y. Y., et al. (2025). In-situ observation of hydrated carbonate in Jezero Crater, Mars. In *56th Lunar and Planetary Science Conference*.

Stack, K. M., Ives, L. R. W., Gupta, S., Lamb, M. P., Tebolt, M., Caravaca, G., et al. (2024). Sedimentology and stratigraphy of the Shenandoah Formation, Western Fan, Jezero Crater, Mars. *Journal of Geophysical Research: Planets*, *129*(2), e2023JE008187. https://doi.org/10.1029/2023JE008187

Stack, K. M., Williams, N. R., Calef, F., III, Sun, V. Z., Williford, K. H., Farley, K. A., et al. (2020). Photogeologic map of the perseverance rover field site in Jezero Crater constructed by the Mars 2020 science team. *Space Science Reviews*, *216*(8), 127. https://doi.org/10.1007/s11214-020-00739-x

Stopar, J. D., Taylor, G. J., Hamilton, V. E., & Browning, L. (2006). Kinetic model of olivine dissolution and extent of aqueous alteration on Mars. *Geochimica et Cosmochimica Acta*. https://doi.org/10.1016/j.gca.2006.07.039

Sun, V. Z., Hand, K. P., Stack, K. M., Farley, K. A., Simon, J. I., Newman, C., et al. (2023). Overview and results from the Mars 2020 perseverance Rover's first science campaign on the Jezero Crater floor. *Journal of Geophysical Research: Planets*. https://doi.org/10.1029/2022JE007613

Tarnas, J. D., Stack, K. M., Parente, M., Koeppel, A. H. D., Mustard, J. F., Moore, K. R., et al. (2021). Characteristics, origins, and biosignature preservation potential of carbonate-bearing rocks within and outside of Jezero Crater. *Journal of Geophysical Research: Planets*, *126*(11), e2021JE006898. https://doi.org/10.1029/2021JE006898

Thorpe, M. T., Bristow, T. F., Rampe, E. B., Tosca, N. J., Grotzinger, J. P., Bennett, K. A., et al. (2022). Mars science laboratory CheMin data from the Glen Torridon Region and the significance of lake-groundwater interactions in interpreting mineralogy and sedimentary history. *Journal of Geophysical Research: Planets*, *127*(11), e2021JE007099. https://doi.org/10.1029/2021JE007099

Tice, M., Hurowitz, J. A., Allwood, A. C., Jones, M. W. M., Orenstein, B. J., Davidoff, S., et al. (2022). Alteration history of Seitah formation rocks inferred by PIXL X-ray fluorescence, X-ray diffraction and multispectral imaging on Mars. *Science Advances*, *8*(47), eabp9084. https://doi.org/10.1126/sciadv.abp9084

Tice, M., Hurowitz, J., Siebach, K., Moreland, E., Kizovski, T. V., Schmidt, M. E., et al. (2024). Regional paleoenvironments recorded in sedimentary rocks of the Western Fan—Delta, Jezero Crater, Mars. In *55th Lunar and Planetary Science Conference*.

Tornabene, L. L., Moersch, J. E., McSween, H. Y. Jr., Hamitlon, V. E., Piatek, J. L., & Christensen, P. R. (2008). Surface and crater-exposed lithologic units of the Isidis Basin as mapped by coanalysis of THEMIS and TES derived data products. *Journal of Geophysical Research*, *113*(E10). https://doi.org/10.1029/2007JE002988

Tosca, N. J., Ahmed, I. A. M., Tutolo, B. M., Ashpitel, A., & Hurowitz, J. A. (2018). Magnetite authigenesis and the warming of early Mars. *Nature Geoscience*, *11*(9), 635–639. https://doi.org/10.1038/s41561-018-0203-8

Tutolo, B. M., Hausrath, E. M., Kite, E. S., Rampe, E. B., Bristow, T., Downs, R. T., et al. (2025). Carbonates identified by Curiosity rover indicate a carbon cycle operated on ancient Mars. *Science*, *388*(6744), 292–297. https://doi.org/10.1126/science.ado9966

Tutolo, B. M., Hausrath, E. M., Rampe, E. B., Bristow, T. F., Downs, R. T., Kite, E., et al. (2024). In situ evidence for an active carbon cycle on ancient Mars. In *55th Lunar and Planetary Science Conference*.

Udry, A., Beyssac, O., Forni, O., Clavé, E., Dehouck, Ostwald, A., et al. (2024). Igneous processes at Jezero Crater and comparison to other Martian igneous compositions. In *Tenth international conference on Mars*.

Udry, A., Ostwald, A., Sautter, V., Cousin, A., Beyssac, O., Forni, O., et al. (2023). A Mars2020 perseverance SuperCam perspective on the igneous nature of the Maaz formation at Jezero Crater and link with Seitah, Mars. *Journal of Geophysical Research: Planets*, *128*(7), e2022JE007440. https://doi.org/10.1029/2022JE007440

Villette, J., Mangold, N., Conway, S. J., Le Deit, L., & Kite, E. S. (2024). The evolution of Pliva Vallis, the outlet valley of the Jezero's Crater lake. In *Tenth international conference on Mars*.

Viviano-Beck, C. E., Seelos, F. P., Murchie, S. L., Kahn, E. G., Seelos, K. D., Taylor, H. W., et al. (2014). Revised CRISM spectral parameters and summary products based on the currently detected mineral diversity on Mars. *Journal of Geophysical Research: Planets*, *119*(6), 1403–1431. https://doi.org/10.1002/2014JE004627

Wells, R. K., Xiong, W., Sesti, E., Cui, J., Giammar, D., Skemer, P., et al. (2017). Spatially-variable carbonate reactions in polycrystalline olivine. *Geochimica et Cosmochimica Acta*, *204*, 252–266. https://doi.org/10.1016/j.gca.2017.02.003

Wieczorek, M. A., Broquet, A., Mclennan, S. M., Rivoldini, A., Glombek, M., Antonangeli, D., et al. (2022). InSight constraints on the global character of the Martian crust. *Journal of Geophysical Research: Planets*, *127*(5), e2022JE007298. https://doi.org/10.1029/2022JE007298

Wiens, R. C., Maurice, S., Robinson, S. H., Nelson, A. E., Cais, P., Bernardi, P., et al. (2021). The SuperCam instrument suite on the NASA Mars 2020 rover: Body unit and combined system tests. *Space Science Reviews*, *217*(1), 4. https://doi.org/10.1007/s11214-020-00777-5

Wiens, R. C., Udry, A., Beyssac, O., Quantin-Nataf, C., Mangold, N., Cousin, A., et al. (2022). Compositionally and density stratified igneous terrain in Jezero Crater, Mars. *Science Advances*, *8*(34), eabo3399. https://doi.org/10.1126/sciadv.abo3399

Williams, A. J., Russell, P. S., Sun, S. Z., Shuster, D., Stack, K. M., Farley, K. A., et al. (2023). Exploring the Jezero Delta front: Overview of results from te Mars 2020 perseverance rover's second science campaign. In *54th Lunar and Planetary Science Conference*.

Williford, K., Farley, K. A., Horgan, B. H. N., Garczynski, B., Treiman, A. H., Gupta, S., et al. (2026). Carbonated ultramafic igneous rocks in Jezero Crater. *Science*, *391*(6787), eadu8264. https://doi.org/10.1126/science.adu8264

Wordsworth, R., Ehlmann, B. L., Forget, F., Haberle, R., Head, J., & Kerber, L. (2018). Healthy debate on early Mars. *Nature Geoscience*, *11*(12), 888. https://doi.org/10.1038/s41561-018-0267-5

Wray, J. J., Murchie, S. L., Bishop, J. L., Ehlmann, B. L., Milliken, R. E., Wilhelm, M. B., et al. (2016). Orbital evidence for more widespread carbonate-bearing rocks on Mars: More widespread carbonate rocks on Mars. *Journal of Geophysical Research: Planets*, *121*(4), 652–677. https://doi.org/10.1002/2015JE004972

Zastrow, A. M., & Glotch, T. D. (2021). Distinct carbonate lithologies in Jezero Crater, Mars. *Geophysical Research Letters*, *48*(9), e2020GL092365. https://doi.org/10.1029/2020GL092365

References From the Supporting Information

Anderson, D. E., Ehlmann, B. L., Forni, O., Clegg, S. M., Cousin, A., Thomas, N. H., et al. (2017). Characterization of LIBS emission lines for the identification of chlorides, carbonates, and sulfates in salt/basalt mixtures for the application to MSL ChemCam data. *Journal of Geophysical Research: Planets*, *122*(4), 744–770. https://doi.org/10.1002/2016JE005164

Anderson, R. B., Gabriel, T. S. J., Seel, F., Clavé, E., Pilleri, P., Clegg, S., et al. (2025). Toward an updated SuperCam LIBS Major Element Quantification. In *56th Lunar and Planetary Science Conference*.

Beck, P., Fau, A., Meslin, P.-Y., Forni, O., & Lasue, J. (2017). Searching for carbon on Mars with MSL ChemCam.

Bernard, S., Beyssac, O., Manrique, J. A., Lopez-Reyes, G., Ollila, A. M., Le Mouélic, S., et al. (2024). Ageing of organics at the surface of Mars: A Raman study aboard perseverance. *Geochemical Perspectives Letters*, *34*, 25–30. https://doi.org/10.7185/geochemlet.2509

Buz, J., & Ehlmann, B. L. (2014). Effects of grain size on the reflectance spectroscopy of olivine in the VIS-NIR and the derivation of olivine composition using modified Gaussian modelling. In *45th Lunar and Planetary Science Conference*.

Chen, F., Sun, C., Qu, S., Zhang, B., Rao, Y., Sun, T., et al. (2024). Determination of inorganic and organic carbons in a Martion soil simulant under the Martian CO_2 atmosphere using LIBS coupled with machine learning. *Spectrochimica Acta Part B: Atomic Spectroscopy*, *214*, 106887. https://doi.org/10.1016/j.sab.2024.106887

Clavé, E., Beyssac, O., Bernard, S., Royer, C., Lopez-Reyes, G., Schroder, S., et al. (2024). Radiation-induced alteration of apatite on the surface of Mars: First in situ observations with SuperCam Raman onboard perseverance. In *Scientific reports*. https://doi.org/10.1038/s41598-024-61494-5

Cousin, A., Forni, O., Maurice, S., Gasnault, O., Fabre, C., Sautter, V., et al. (2011). Laser induced breakdown spectroscopy library for the Martian environment. *Spectrochimica Acta Part B: Atomic Spectroscopy*, *66*(11–12), 805–814. https://doi.org/10.1016/j.sab.2011.10.004

Cristoforetti, G., De Giacomo, A., Dell'Aglio, M., Legnaioli, S., Tognoni, E., Palleschi, V., & Omenetto, N. (2010). Local thermodynamic equilibrium in laser-induced breakdown spectroscopy: Beyond the McWhirter criterion. *Spectrochimica Acta Part B: Atomic Spectroscopy*, *65*(1), 86–95. https://doi.org/10.1016/j.sab.2009.11.005

Guezenoc, J., Gallet-Budynek, A., & Bousquet, B. (2019). Critical review and advices on spectral-based normalization methods for LIBS quantitative analysis. *Spectrochimica Acta, Part B: Atomic Spectroscopy*, *160*, 105688. https://doi.org/10.1016/j.sab.2019.105688

King, T. V. V., & Ridgly, W. I. (1987). Relation of the spectroscopic reflectance of olivine to mineral chemistry and some remote sensing implications. *Journal of Geophysical Research*, *92*(B11), 11457–11469. https://doi.org/10.1029/JB092iB11p11457

Kramida, A., Ralchenko, Y., & Reader, J., & NIST Atomic Spectra Database Team. (2022). NIST Atomic Spectra Database (version 5.10). https://doi.org/10.18434/T4W30F

Manrique, J. A., Lopez-Reyes, G., Cousin, A., Rull, F., Maurice, S., Wiens, R. C., et al. (2020). SuperCam calibration targets: Design and development. *Space Science Reviews*, *216*(8), 138. https://doi.org/10.1007/s11214-020-00764-w

Montagnac, G., Dromart, G., Beck, P., Mercier, F., Reynard, B., Cousin, A., et al. (2018). Spark plasma sintering preparation of reference targets for field spectroscopy on Mars. *Journal of Raman Spectroscopy*, *49*(9), 1419–1425. https://doi.org/10.1002/jrs.5406

Ollila, A. M., Blank, J. G., Wiens, R. C., Lasue, J., Newsom, H. E., Clegg, S. M., et al. (2011). Preliminary results on the capabilities of the ChemCam lase-induced breakdown spectroscopy (LIBS) instrument to detect carbon on Mars. In *42nd Annual Lunar and Planetary Science Conference* (p. 2395).

Sahal-Bréchot, S., Dimitrijević, M. S., Moreau, N., & Ben Nessib, N. (2013). STARK-B: Database for Stark broadening of isolated lines of atoms and ions in the impact approximation.

Ytsma, C. R., & Dyar, M. D. (2019). Accuracies of lithium, boron, carbon, and sulfur quantification in geological samples with laser-induced breakdown spectroscopy in Mars, Earth, and vacuum conditions. *Spectrochimica Acta Part B: Atomic Spectroscopy*, *162*, 105715. https://doi.org/10.1016/j.sab.2019.105715